

# The Importance of Lake Emergent Aquatic Vegetation for Estimating Arctic-Boreal Methane Emissions

Ethan D. Kyzivat<sup>1</sup>, Laurence C. Smith<sup>1</sup>, Fenix Garcia-Tigreros<sup>2</sup>, Chang Huang<sup>1,3</sup>, Chao Wang<sup>4</sup>, Theodore Langhorst<sup>4</sup>, Jessica V. Fayne<sup>5</sup>, Merritt E. Harlan<sup>6</sup>, Yuta Ishitsuka<sup>6</sup>, Dongmei Feng<sup>10</sup>, Wayana Dolan<sup>4</sup>, Lincoln H Pitcher<sup>5,8</sup>, Kimberly P. Wickland<sup>7</sup>, Mark M. Dornblaser<sup>7</sup>, Robert G. Striegl<sup>7</sup>, Tamlin M. Pavelsky<sup>4</sup>, David E. Butman<sup>2,9</sup>, and Colin J. Gleason<sup>6</sup>

<sup>1</sup>Department of Earth, Environmental & Planetary Sciences and Institute at Brown for Environment & Society, Brown University, Providence, RI, 02912 USA

<sup>2</sup>School of Environmental and Forest Sciences, University of Washington, Seattle, WA, 98195 USA

<sup>3</sup>School of Urban and Environmental Sciences, Northwest University, Xi'an, Shaanxi, 710127 China

<sup>4</sup>Department of Earth, Marine and Environmental Sciences, University of North Carolina, Chapel Hill, NC, 27599 USA

<sup>5</sup>Department of Geography, University of California-Los Angeles, Los Angeles, CA, 90095 USA

<sup>6</sup>Department of Civil and Environmental Engineering, University of Massachusetts, Amherst, MA, 01003 USA

<sup>7</sup>U.S. Geological Survey, Water Resources Mission Area, Boulder, CO, 80303 USA

<sup>8</sup>Cooperative Institute for Research in Environmental Sciences (CIRES). University of Colorado, Boulder. Boulder, CO, 80309, USA.

<sup>9</sup>School of Engineering and Environmental Sciences, University of Washington, Seattle, WA, 98195 US

<sup>10</sup>Department of Chemical and Environmental Engineering, University of Cincinnati, OH, 45221 USA

Corresponding author: Ethan D. Kyzivat ([ethan.kyzivat@aya.yale.edu](mailto:ethan.kyzivat@aya.yale.edu))

## Key Points:

- We provide a first quantification of emergent vegetation area across 4,572 lakes in four Arctic-boreal study areas using airborne mapping.
- Lake emergent vegetation coverage varies regionally from 1 to 59 percent of lake area and seasonally to a lesser degree.
- Accounting for this coverage could increase Arctic-boreal lake methane upscaling estimates by 21 percent.

## 36 **Abstract**

37 Areas of lakes that support emergent aquatic vegetation emit disproportionately more methane  
38 than open water but are under-represented in upscaled estimates of lake greenhouse gas  
39 emissions. These shallow areas are typically less than ~1.5 m deep and can be estimated through  
40 synthetic aperture radar (SAR) mapping. To assess the importance of lake emergent vegetation  
41 (LEV) zones to landscape-scale methane emissions, we combine airborne SAR mapping with  
42 field measurements of vegetated and open-water methane flux. First, we use Uninhabited Aerial  
43 Vehicle SAR (UAVSAR) data from the NASA Arctic-Boreal Vulnerability Experiment  
44 (ABoVE) to map LEV in 4,572 lakes across four Arctic-boreal study areas and find it comprises  
45 ~16% of lake area, exceeding previous estimates, and exhibiting strong regional differences  
46 (averaging 59 [50–68]%, 22 [20-25]%, 1.0 [0.8-1.2]%, and 7.0 [5.0-12]% of lake areas in the  
47 Peace-Athabasca Delta, Yukon Flats, and northern and southern Canadian Shield, respectively).  
48 Next, we account for these vegetated areas through a simple upscaling exercise using paired  
49 methane fluxes from regions of open water and LEV. After excluding vegetated areas that could  
50 be accounted for as wetlands, we find that inclusion of LEV increases overall lake emissions by  
51 21 [18-25]% relative to estimates that do not differentiate lake zones. While LEV zones are  
52 proportionately greater in small lakes, this relationship is weak and varies regionally,  
53 underscoring the need for methane-relevant remote sensing measurements of lake zones and a  
54 consistent criterion for distinguishing wetlands. Finally, Arctic-boreal lake methane upscaling  
55 estimates can be improved with more measurements from all lake zones.

56

## 57 **Plain Language Summary**

58 Lakes are one of the largest natural sources of the greenhouse gas methane and are especially  
59 common in high latitudes. Shallow, near-shore areas of lakes having emergent aquatic vegetation  
60 emit disproportionately more methane than open water areas but are under-represented in broad-  
61 scale estimates of lake greenhouse gas emissions. While lake depths are difficult to map from  
62 remote sensing, emergent vegetation, which typically grows in water less than ~ 1.5 m deep, can  
63 be detected via radar remote sensing. To assess the importance of these areas to landscape-scale  
64 methane emissions, we combine airborne radar mapping with field measurements of vegetated  
65 and open-water methane emissions. Zones of emergent vegetation vary regionally and comprise  
66 ~16% of lake area on average. A simple estimate that accounts for both open water and emergent  
67 vegetation methane emissions results in 21% increased overall lake methane emissions estimates.  
68 Emergent aquatic vegetation coverage has only a weak relationship with lake size, making it  
69 hard to predict. Therefore, to better estimate broad-scale methane emissions, we suggest using  
70 remote sensing to create lake vegetation distribution maps and measuring methane emissions  
71 from both vegetated and open water zones within lakes.

72

## 73 **1 Introduction**

74 Inland waters (lakes, reservoirs, rivers, and wetlands) are the single largest natural source  
75 of the greenhouse gas methane (CH<sub>4</sub>) (Saunois et al., 2020). Lakes are estimated to be  
76 responsible for ~24% of all inland water emissions, second only to wetlands (Bastviken et al.,  
77 2011; Saunois et al., 2020). They emit methane via diverse pathways of diffusion, ebullition,

78 transport through aquatic plant tissue, and through a storage flux during turnover and/or ice melt  
79 in stratified lakes. Emissions are strongly dependent on temperature, sediment carbon content,  
80 redox environment, and gas transfer velocity (Bastviken, Cole, Pace, & Tranvik, 2004; Wik et  
81 al., 2016). Uncertainties in upscaling lake emissions therefore have vast spatial and temporal  
82 heterogeneities (Loken et al., 2019; Natchimuthu et al., 2016; Stephanie et al., 2020; Saunio et  
83 al., 2020).

84 Unlike for wetlands, there are few process-based models for lake fluxes, so estimates  
85 have relied on data-driven extrapolations (Saunio et al., 2020). Lake emission upscaling efforts  
86 have only recently begun to account for lake surface area (DelSontro et al., 2016; Hastie et al.,  
87 2018; Holgerson & Raymond, 2016), but it is still rare to consider other aspects of morphometry,  
88 such as slope, vegetation, and littoral area (Casas-Ruiz et al., 2021). “Bottom-up,” or process-  
89 based, methane estimates tend to over-predict aquatic methane fluxes compared to “top-down,”  
90 or inversion-based, models (Saunio et al., 2020), and double-counting of small lakes as  
91 wetlands caused by mismatch in scale and methods among datasets has been suggested as a  
92 possible cause (Thornton et al., 2016). Small ( $< 0.001 \text{ km}^2$ ) lakes and wetlands are poorly  
93 mapped, especially in Arctic-boreal regions containing the world’s greatest abundance of lakes  
94 (Verpoorter et al., 2014). Indeed, uncertainty in wetland extent is frequently cited as the leading  
95 cause of uncertainty in bottom-up methane estimates (Zhang et al. 2017), and errors arising from  
96 large-scale extrapolations of heterogeneous wetlands have also been noted (Bridgman et al.,  
97 2013).

98 One key challenge to upscaling is the high within-lake spatial variability of methane  
99 emissions. Total fluxes measured from vegetated (Villa et al., 2021) and shallow (Natchimuthu  
100 et al., 2016) zones can be statistically greater than those from open water and have been  
101 attributed to the majority of whole-lake emissions (Saunio et al., 2020). Estimates derived from  
102 deep lake centers have been shown to underestimate total flux by 5-78% in select lakes  
103 (Natchimuthu et al., 2016). Plant-mediated fluxes can be significant at the landscape scale, for  
104 example exceeding peatland emissions in southern Finland by 30%, despite covering only 40%  
105 as much area (Bergström et al., 2007). Another study of three Finnish lakes found that the  
106 vegetated littoral zone produced 66-77% of whole-lake emissions (Juutinen et al., 2003).  
107 Combined globally, emergent macrophytes are estimated to emit 11% of the equivalent from all  
108 open water lakes, rivers, and reservoirs (Bastviken et al., 2011). As the most “wetland-like” zone  
109 within lakes, littoral zones are important sources of carbon and known methane emission hot  
110 spots (Bergström et al., 2007; Burger et al., 2016; Huttunen et al., 2003; Juutinen et al., 2003;  
111 Larmola et al., 2004), with exceptions (Jansen et al., 2020a). However, littoral zone area is  
112 difficult to quantify accurately because its extent is classified by light penetration into the water  
113 column (Wetzel, 2001) and not by characteristics that are easily delineated by remote sensing. In  
114 contrast, the extent of emergent macrophytes growing in water  $< \sim 1.5 \text{ m}$  deep in the upper  
115 littoral zone are more easily detected. These plants can act as conduits to the atmosphere for  
116 methane produced in lake sediments (Dacey and Klug, 1979; Colmer, 2003). They also produce  
117 carbon compounds that are preferentially consumed by methanogens (methane-producing  
118 archaea), and their decomposing biomass and root exudates are a large contributor to sediment  
119 organic carbon (Christensen et al., 2003; Joabsson, Christensen, & Wallén, 1999; Ström et al.,  
120 2005). Previous studies have noted the tendency for small (Michmerhuizen, Striegl, &  
121 McDonald, 1996; Bastviken et al., 2004; Holgerson & Raymond, 2016; Engram et al. 2020) and  
122 shallow (West et al., 2015; Wik et al., 2016a; Li et al., 2020) lakes to emit more methane than  
123 larger and deeper ones. DelSontro et al. (2018b) successfully modeled lake methane

124 concentration as a function of distance from the littoral zone, horizontal transport and oxidation,  
125 and oxic epilimnetic production, which highlights the outsized importance of littoral methane  
126 production. Notably, not all properties of littoral zones come from their vegetation. Their relative  
127 shallowness is also a factor, as depth often prohibits methane ebullition due to water overburden  
128 pressure (Bastviken et al., 2004, Langenegger et al., 2019), although there are exceptions  
129 (Huttunen et al., 2003). Shallow waters may also contain distinct sediment organic matter  
130 composition and less opportunity for microbe-mediated oxidation of dissolved methane  
131 (DelSontro et al., 2016). Finally, diffusive fluxes measured in the littoral zone may be driven by  
132 terrestrial inflows (Paytan et al., 2015, Natchimuthu et al., 2016), and offshore fluxes are  
133 diminished by oxidation during transport (DelSontro et al., 2018b). Thus, methane emissions in  
134 lakes are spatially variable, with highest emissions coming from littoral zones, particularly with  
135 vegetation.

136 This challenge of accounting for spatial heterogeneity is exacerbated by lack of data in  
137 the littoral or vegetated zones (DelSontro et al. 2018b; Desrosiers et al., 2022). The Boreal–  
138 Arctic Wetland and Lake Methane Dataset (BAWLD-CH<sub>4</sub>; Kuhn et al., 2021a; Kuhn et al.,  
139 2021b) is the first synthesis study we are aware of that notes which part of the lake ebullition  
140 fluxes were measured (center, edge, or whole lake). However, only 143 of the 553 records  
141 actually contain within-lake location, and of these, only one was measured from an edge, with 19  
142 from centers and 123 from whole-lakes. Among lake methane studies, plant-mediated emissions  
143 are measured least frequently of all lake pathways (Bastviken et al., 2011; Wik et al., 2016a),  
144 along with open-water emissions near plants, so methane upscaling estimates in lakes (DelSontro  
145 et al., 2018a; Tranvik et al., 2009) usually rely solely on pelagic diffusion and ebullition  
146 (DelSontro et al. 2018; Desrosiers et al., 2021), with biases introduced by insufficient within-  
147 lake sampling sites (Wik et al., 2016b). For these reasons, lake methane measurements are under-  
148 represented in vegetated and littoral zones, even among the few studies that report sampling  
149 location.

150 Another key challenge to upscaling is that littoral and vegetation coverage in lakes are  
151 poorly constrained. Duarte et al. (1986) suggested that emergent macrophytes colonize on  
152 average 7% of a lake regardless of its area, while submerged macrophyte coverage generally  
153 declines with area. They list light availability, sediment characteristics, and trophic status as key  
154 characteristics for macrophyte growth, with slope as the greatest predictor of emergent  
155 macrophyte coverage. Others have theorized that the percent of a lake's surface area covered  
156 with macrophytes scales with nitrogen concentration and the inverse of mean depth (Smith and  
157 Wallsten 1986), or scales inversely with lake area (Michmerhuizen et al., 1996) or perimeter  
158 (Bergström et al., 2007). Mäkelä et al. (2004) similarly found that an average of 6% (range: 1-  
159 100%) of total lake area was covered by macrophytes in a sample of 50 lakes and that total  
160 fractional macrophyte coverage per lake steeply declined with lake area. Zhang et al. (2017)  
161 compiled a synthesis database of aquatic macrophytes in 155 global lakes and observed an  
162 average coverage of 26% (range: 0.000-100%) with an accelerating decline since 1900.

163 Remote sensing studies have used both optical and synthetic aperture radar (SAR)  
164 sensors to map macrophytes in lakes. Optical satellites are better suited to detecting vegetation  
165 type, while SAR can detect water even through vegetation canopies (Hess et al., 1990). Ghirardi  
166 et al. (2019) used optical Sentinel-2 satellite data to map submerged aquatic macrophytes in an  
167 Italian lake and noted both inter- and intra-annual variations in aerial coverage. Nelson et al.  
168 (2006) used Landsat Thematic Mapper imagery to map various types of macrophytes in 13 lakes

169 in Michigan, USA and found total macrophyte coverage ranging from 5-42%. Ganju et al. (2017)  
170 used air imagery and elevation data to derive the unvegetated/vegetated marsh ratio (UVVR) for  
171 tidal marshes, which scales with sediment budget and has typical values  $< 0.4$ . Zhang et al.  
172 (2018) used TerraSAR-X SAR imagery to map macrophytes in nine Brazilian reservoirs and  
173 similarly found large spatial and temporal variation in coverage. Thus, many remote sensing  
174 studies have demonstrated spatial and/or temporal differences in aquatic macrophyte cover, yet  
175 few have measured total coverage across large geographical areas and numerous lakes. Lake  
176 macrophyte area statistics, therefore, remain confined to a handful of studies of small numbers of  
177 lakes.

178 Here, we aim to quantify the fractional coverage of emergent vegetation for 4,572 lakes  
179 across four Arctic-boreal regions in order to assess their potential importance in scaling methane  
180 emissions. To estimate coverage, we use the canopy-penetrating properties of L-band synthetic  
181 aperture radar (SAR) flown during the NASA Arctic-Boreal Vulnerability Experiment (ABoVE)  
182 airborne campaign (2017-2019). Although floating-leafed macrophytes are relevant to the  
183 methane budget, they cannot be reliably detected with this technique due to similar surface  
184 roughness with water waves and thus are omitted here. Next, we compile paired measurements  
185 of methane flux (new data and literature) via all pathways from open water and emergent  
186 macrophyte regions of lakes. Finally, we use these flux measurements and our remote sensing-  
187 derived ranges in emergent vegetation coverage to estimate its impact on lake methane  
188 emissions. We conclude with discussion of the causes of regional differences, some broader  
189 recommendations for landscape-scale methane upscaling, study limitations, and  
190 recommendations for future research.

## 191 **2 Study areas, data sources, and methods**

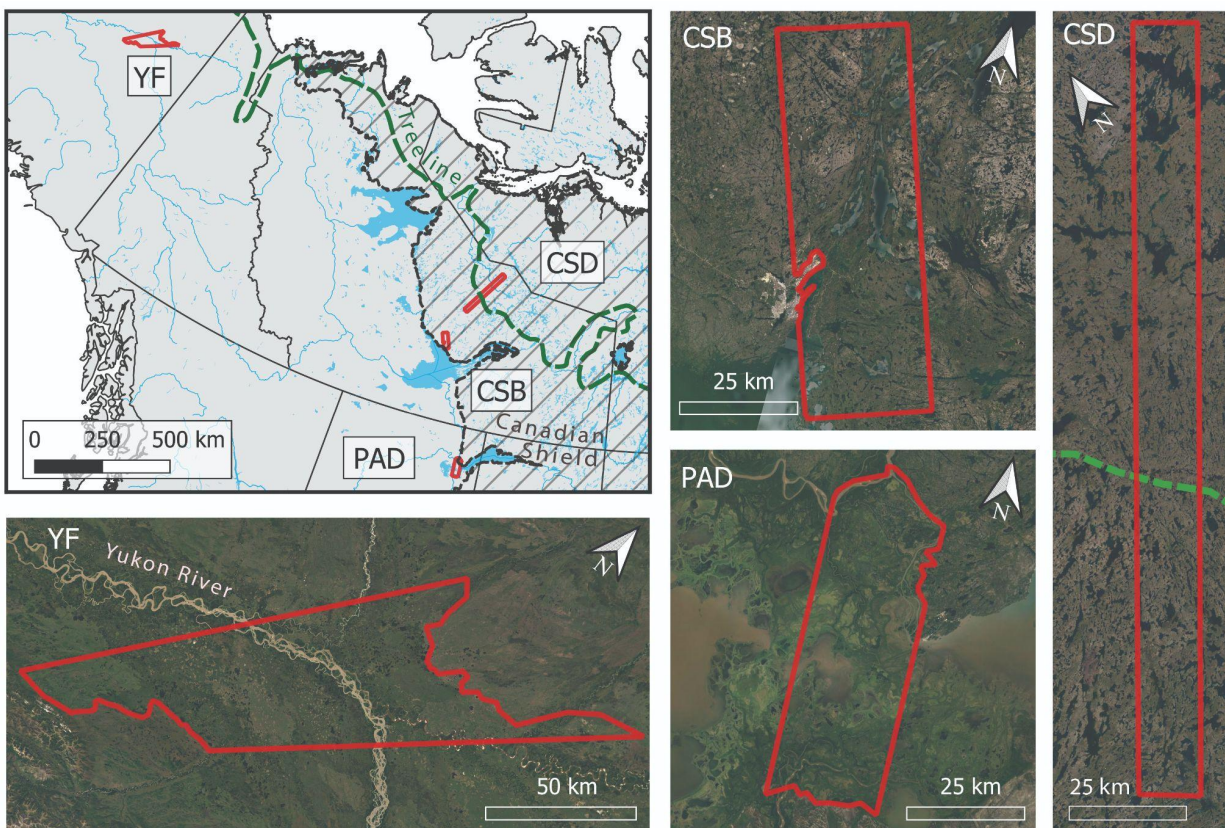
### 192 **2.1 Study areas**

193 The NASA Arctic-Boreal Vulnerability Experiment (ABoVE) campaign is a decade-long  
194 effort to measure environmental change in the Arctic and boreal regions of western North  
195 America via coordinated ground measurements and airborne remote sensing (Miller et al., 2019).  
196 Here, we focus on four study areas within the ABoVE domain, each corresponding to one or  
197 more flight lines from its airborne campaigns:

- 198 1) Peace-Athabasca Delta, Alberta, Canada (PAD);
- 199 2) Southern Canadian Shield near Baker Creek (CSB), Northwest Territories, Canada;
- 200 3) Interior Canadian Shield near Daring Lake (CSD), Northwest Territories, Canada; and
- 201 4) Yukon Flats National Wildlife Refuge, Alaska, USA (YF).

202 These four study areas were chosen because of their high lake density and contrasting geological,  
203 hydrological, and ecological conditions. The PAD is one of the world's largest inland deltas and  
204 is located on the western edge of Lake Athabasca (**Figure 1**). The overall relief of its lowland  
205 regions is 11 m, causing numerous marsh-type wetlands, mudflats, and lakes, many of which are  
206 recharged by the Athabasca River (Pavelsky & Smith, 2008), and more rarely, by ice-jam floods  
207 in the Peace River (Timoney, 2013). These floods can inundate up to 80% of the 5,600 km<sup>2</sup> delta  
208 (Töyrä & Pietroniro, 2005; Wolfe et al., 2006), while in typical years, 26% is covered by  
209 intermittently-inundated wetlands (Ward & Gorelick 2018). It is a Ramsar Wetland, UNESCO  
210 World Heritage site, and home to numerous endemic species of birds, fish, and mammals

211 including the endangered whooping crane and the largest remaining herd of wood bison (Parks  
 212 Canada, 2019). The two Northwest Territories study areas (CSD, CSB) are located on the  
 213 Canadian Shield, the world's largest deposit of Precambrian-age bedrock and source of the oldest  
 214 known terrestrial rocks (Slaymaker, 2016). Deglaciated only nine thousand years ago and with a  
 215 rocky, sparse surface drainage pattern, the Shield is also the world's most lake-rich region and  
 216 contains many peatlands (Slaymaker, 2016; Spence & Woo, 2006). CSB is underlain by  
 217 discontinuous permafrost, while CSD crosses the tree line and contains a transition to continuous  
 218 permafrost and the tundra/taiga ecotone (**Figure 1**). The YF is underlain by discontinuous  
 219 permafrost in alluvial soils and contains lakes of various hydrologic connectivity to the Yukon  
 220 River and its tributaries (Anderson et al. 2013, Johnston et al., 2020). Like the PAD, the YF has  
 221 flat topography, permitting seasonal flooding during the early summer to cover large areas, and it  
 222 is a source of both lateral riverine and water-air carbon fluxes (Striegl, et al., 2012). All four  
 223 study areas are home to multiple indigenous and First Nation communities, as well as the city of  
 224 Yellowknife (CSB) and numerous smaller settlements.



225

226 **Figure 1.** Location map of study areas (YF = Yukon Flats; CSD = Canadian Shield, Daring  
 227 Lake; CSB = Canadian Shield, Baker Creek; PAD = Peace-Athabasca Delta). Study area  
 228 boundaries (red polygons) are derived from intersecting UAVSAR airborne flight coverage with  
 229 physiographic boundaries. Major water bodies are shown in blue; Canadian Shield with  
 230 stippling, and the northern tree line limit (Brown et al., 2002) in green.

231

## 232 2.2 Data sources

## 233 2.2.1 Airborne polarimetric SAR

234 L-band synthetic aperture radar (SAR) data from the Uninhabited Aerial Vehicle  
 235 Synthetic Aperture Radar (UAVSAR) were obtained in multi-look ground-projected format  
 236 (GRD) and reprojected to ~5.5 m spatial resolution (NASA/JPL 2017-2019) on the ABoVE  
 237 Science Cloud computing environment. With a wavelength of 23.8 cm, UAVSAR has been used  
 238 extensively for vegetation mapping and inundation detection, including in lowlands or deltas  
 239 with flooded vegetation (Ayoub et al., 2018; Jensen et al., 2021; Z. Zhang et al., 2017). All  
 240 available ABoVE UAVSAR flight dates from non-contiguous days during summers 2017-2019  
 241 were used. Both early (June) and late (August-September) summer images were acquired by  
 242 UAVSAR in 2017, and only late summer/early autumn dates were imaged in 2018 and 2019.

243

## 244 2.2.2 Water and land cover maps

245 Several ABoVE land cover data sets were referenced to help build a land cover training dataset  
 246 for UAVSAR (see **Section 2.3.1**). High-resolution imagery and derivative water masks were  
 247 obtained from the AirSWOT color-infrared camera (Kyzivat et al. 2018; Kyzivat et al. 2019;  
 248 Kyzivat, et al. 2020), supplemented by high-resolution satellite imagery from Maxar  
 249 (<https://evwhs.digitalglobe.com/myDigitalGlobe/>). Two satellite-based land cover maps  
 250 available for the ABoVE domain were also referenced (Bourgeau-Chavez et al., 2017, 2019;  
 251 Wang et al., 2019; Wang et al., 2019). Although these maps use a different classification scheme  
 252 than our derived UAVSAR classification, they are particularly useful for partitioning between  
 253 trees, shrubs, and graminoid vegetation.

254

## 255 2.3 Methods

## 256 2.3.1 Land cover classification training dataset

257 To estimate lake emergent macrophyte coverage ( $A_{EV}$ ), a land cover training dataset was  
 258 created using inundation status from field measurements in 2015 and 2017-2019 and vegetation  
 259 categories from ABoVE land cover maps (Bourgeau-Chavez et al., 2017, 2019; Wang et al.,  
 260 2019; Wang et al., 2019). As part of the field measurements, lake and wetland shorelines and  
 261 vegetation zones were mapped by field teams carrying handheld GPS receivers, as described in  
 262 Kyzivat et al. (2019). In YF, airborne GPS tracks from a low-hovering helicopter were used, as  
 263 no suitable ground GPS tracks were available. Contextual photos were also taken by camera,  
 264 both from the ground and from aircraft windows, and by uninhabited airborne vehicles (UAVs).  
 265 UAV photos were processed into orthomosaics using DroneDeploy web software. All of these  
 266 measurements were digitized into polygon shapefiles in ArcGIS 10.6 denoting 13 land cover  
 267 classes falling into five broad categories of open water, dry land and three types of emergent  
 268 vegetation (**Table 1**). The resulting vector data set was used to train and validate a supervised  
 269 classification from the radar data (Kyzivat et al., 2021a).

270

Broad Grouping	UAVSAR land cover class
----------------	-------------------------

Open surface water	Open Water (OW), Rough Water (RW), Sedimentary Bar (SB), Wet Herbaceous (WH)
Wet Graminoid	Wet Graminoid (WG)
Wet Shrub	Wet Shrub (WS)
Wet Forest	Wet Forest (WF)
Dry land	Dry Graminoid (DG), Dry Shrub (DS), Dry Forest (DF), Bank Scarp Double-Bounce (BS), Dry Woodland (DW), Bare Ground (BG)

271 **Table 1.** Classification Schema: RW refers to wind roughening at the time of acquisition. WG  
 272 refers to cattails (*Typha latifolia*), bulrushes (*Scirpus* spp.), and sedges (*Carex* spp.), as well as  
 273 aquatic horsetails (*Equisetum fluviatile*). WS typically refers to willows (*Salix* spp.). DW refers  
 274 to a mix of trees and shrubs as defined by Wang (2019). WH refers to water lilies (*Nuphar*  
 275 *variegatum*), and both WH and SB were not separable from the other open water classes. Further  
 276 details are in the accompanying data publication (Kyzivat et al., 2021a).

277

### 278 2.3.2 Synthetic aperture radar data pre-processing

279 UAVSAR GRD data for the PAD, YF and CSB flight lines were transformed to the C3  
 280 complex covariance matrix using PolSAR Pro 6.0 software. Images were corrected for incidence  
 281 angle-dependent backscatter using a fitted exponential function multiplied by the cosine of  
 282 incidence angle as per Ulander (1996) and Zhang et al. (2017). Due to its more rugged  
 283 topography, CSD was corrected for both incidence angle and terrain slope as per the look-up  
 284 table method of Simard et al. (2016). For all flight lines, a Freeman-Durden polarimetric  
 285 decomposition was performed. The decomposition comprises a physical scattering model and is  
 286 commonly used to identify scattering mechanism contributions to each pixel (single bounce,  
 287 modeled as Bragg scattering; double bounce, modeled as from a pair of orthogonal surfaces; and  
 288 volume scattering, modeled as from a cloud of randomly-oriented dipoles) (Freeman & Durden,  
 289 1998). Although it is known to overestimate the double bounce component (Chen et al., 2014), it  
 290 is sufficient as an input feature to an empirical, machine-learning based classification.

### 291 2.3.3 Land cover classification

292 Each of the three scattering mechanism output bands was used for feature extraction via  
 293 three moving-window filters designed to introduce spatial contextual information for the  
 294 classifier. The chosen filters were standard deviations, offsets oriented along the radar look  
 295 direction, and an edge-preserving guided filter to reduce speckle (**Table S.2**). Additional input  
 296 bands of incidence angle and elevation-derived indexes were tested, but ultimately omitted, due  
 297 to their high spatial autocorrelation, which led to model over-fitting. The training class BS was  
 298 developed specifically to identify bright double bounce scattering between water surfaces and  
 299 steep bank scarps, which would otherwise have appeared as inundated vegetation. SB and WH  
 300 (defined as protruding <20 cm from the water surface, as determined from field measurements)  
 301 were found to be inseparable from OW, so they were treated as open surface water in the  
 302 analysis. The radar dataset was further prepared for classifier training by randomly under-  
 303 sampling the majority training classes and cropping out pixels taken at low incidence angles.

304 Incidence angle limits as well as filter parameters (**Table S.2**) were chosen by trial and error.  
305 Finally, pixel values within training polygons in all input bands from the appropriate date were  
306 extracted, and the results split using stratified sampling into training (85%) and validation (15%)  
307 datasets with 15 bands each. A description of this workflow, parameter settings, and other  
308 technical details is provided in **Table S.2**.

309 Finally, a random forests classifier was trained using the TreeBagger function in  
310 MATLAB R2017b and evaluated using the validation dataset via the confusion matrix and  
311 Cohen's kappa coefficient. One model was used for the areas with incidence angle correction  
312 and another for the CSD area with the look-up table correction. The models were then applied  
313 over the extent of their corresponding study areas for all available dates. The original 13 classes  
314 were aggregated into the five generalized classes for analysis (**Table 1**).

315

#### 316 2.3.4 Quality control and conversion to emergent vegetation coverage

317 The derived five-class land cover maps were used to identify emergent macrophyte and  
318 open water areas and quantify their total landscape coverage. First, maps were clipped to the  
319 intersection of all flight lines per study area excluding any roads or urban areas, if present. Raster  
320 mosaics were created for the PAD and YF, since they were acquired in multiple flight lines on  
321 most dates (**Table S.1**). Next, candidate lakes were identified as connected pixel groups of at  
322 least five pixels with at least one open water pixel and any number of inundated vegetation pixels  
323 (or none at all). This criterion permitted inclusion of open water wetlands, because there is no  
324 reliable way to differentiate them from lakes and ponds. Rivers were removed by applying a  
325 manually-created river mask, modified from Kyzivat et al. (2019). Lake emergent vegetation  
326 ( $A_{LEV}$ ) were operationally defined as emergent vegetation classes 8-connected to lakes, with the  
327 remaining emergent vegetation pixels considered wetlands ( $A_{WEV}$ ). Although dependent on pixel  
328 size, this definition permitted a consistent definition across all study areas. At this stage, the total  
329 landscape coverage of  $A_{LEV}$  (wet graminoid, shrub, and forest classes) and open water were  
330 calculated so they could be compared between dates.

331 Although there is scarce data for methane emission from trees and shrubs along lake  
332 shores, we included them in the sensitivity analysis because: 1) 69% of  $A_{LEV}$  is comprised of  
333 graminoid vegetation and this value increases to >97% after correcting for double counting (see  
334 **3.1.1**); 2) There is no mixed coverage class, meaning there is likely still graminoid vegetation  
335 present, but hard to detect; 3) Data scarcity makes it hard to account for them separately; and 4)  
336 Many of the factors that make vegetated water surfaces high emitters are shared between  
337 vegetation types, such as shallowness, proximity to terrestrial inputs, variable inundation, and  
338 presence of root systems. In fact, these dynamically-inundated water surfaces with woody  
339 vegetation, which could also be called littoral swamps, have been shown to emit methane four  
340 orders of magnitude greater than temperate forest soil uptake (Hondula et al., 2021). This  
341 observation underscores the importance of accounting for regions of emergent lake vegetation  
342 separately from open water, while being sure to exclude any regions otherwise accounted for as  
343 wetlands (see **2.3.7**).

344 To calculate  $A_{LEV}$  coverage on a per-lake basis, water bodies smaller than 250 m<sup>2</sup>  
345 (0.00025 km<sup>2</sup> or 7-8 px) were discarded, since they were too small to consistently resolve and  
346 likely included false detections. Although hardly affecting total lake area, false detections of

347 lakes would be disproportionately small and thus impact the distribution of  $A_{LEV}$ . Partially  
348 observed lakes intersecting the flight line boundary were discarded as well, since  $A_{LEV}$  could not  
349 be reliably measured. A third category of lakes were discarded if they did not overlap with any  
350 water pixels in the 2017 AirSWOT color-infrared camera open water masks, which had a slightly  
351 narrower ground footprint in all study areas. By comparing our UAVSAR retrievals to an  
352 independent, optical data set, this step removed many falsely-identified lakes caused by  
353 classification error. Finally, we calculated the areas of the remaining lakes and the fractional area  
354 of their emergent vegetation ( $A_{LEV}$ ) coverages, defined as the proportion of pixels in a lake  
355 classified as any of the three inundated vegetation classes. For visualization and analysis, these  
356 data were divided into 24 logarithmically-spaced lake area bins across the four study areas, and  
357 the mean, lake area-weighted mean, and median  $A_{LEV}$  computed for each study area. For each  
358 study area, confidence intervals were calculated for each of the 24 bins and for the area-weighted  
359 means using the 95<sup>th</sup> percentile of 10,000 bootstrapped simulated datasets.

360

### 361 2.3.5 Adjusting estimate to avoid double-counting wetlands

362 Our method for detecting emergent vegetation excludes wetlands based on lack of pixel  
363 connectivity to open water. Although this method conserves total area and thus does not double-  
364 count any pixel to more than one land cover class, this partitioning includes open-water and  
365 littoral wetlands as parts of lakes. As a result, our estimate of  $A_{LEV}$  would be too high because it  
366 treats areas typically considered to be wetlands (e.g. in methane models) as parts of lakes, which  
367 is precisely the double-counting between datasets described by Thornton et al. (2016). To correct  
368 for this over-estimate of total lake area, we obtained two leading global lake datasets,  
369 GLOWABO (Verpoorter et al., 2014) and HydroLAKES (Messenger et al., 2016) and compared  
370 total lake extent between the datasets and our own. First, since the global datasets were made at a  
371 coarser geographic scale, USAVSAR lakes below the appropriate minimum size threshold were  
372 excluded (0.002 km<sup>2</sup> for GLOWABO and 0.1 km<sup>2</sup> for HydroLAKES). Even so, there were still  
373 many more lakes detected by UAVSAR (and some only detected by one of the other datasets), so  
374 spatial selection in the python package geopandas 0.10.2 (Jordahl et al., 2021) was used to  
375 exclude any lakes in either dataset that did not overlap at least partly with a lake in the dataset to  
376 which it was being compared. This exclusion ensured that we were only comparing areas within  
377 commonly-detected lakes and not simply assessing lake mapping accuracy between the datasets,  
378 which have vastly different scales and time domains. Next, both datasets were rasterized to the  
379 UAVSAR pixel grid for the corresponding scene, typically 5.5 by 5.5 m pixels. Then, for each  
380 study area, a confusion matrix was computed between the UAVSAR dataset and each of the  
381 others for all pixels not denoted as land in both candidate datasets. These matrices were used to  
382 compute the scalar  $c$ , which is used in **Equation [1]** and denotes how much of UAVSAR  $A_{LEV}$   
383 falls within global dataset lakes, with the remainder assumed to already be mapped as wetlands  
384 with adequate accounting of methane emissions.

385 The calculation ignores the effects of changing inundation during the 10-20 years  
386 between data acquisitions, as well as errors arising from the global datasets having less-precise  
387 georeferencing. It is also limited to only the large lakes that could be compared between datasets.  
388 Since these biases would also exist in any modeling study using GLOWABO or HydroLAKES,  
389 we have made no attempt to correct for them, which would also be beyond the scope of this  
390 work.

### 391 2.3.6 Methane flux chamber measurements

392 24 methane fluxes were measured at 15 lakes in the PAD during July and August 2019  
393 (Kyzivat et al. 2021, **Figure S.6**). The sampling schedule permitted no more than one or two  
394 visiting days per lake, so the measurements represent a broad, geographic sampling within the  
395 PAD at the expense of frequent measurements in any one lake. This sampling approach allowed  
396 for better, but still limited extrapolation to the 470 UAVSAR-observed lakes in the PAD. In all  
397 15 lakes, single 15-minute fluxes were taken from an open water region near the lake center via  
398 inflatable raft, anchored canoe, or motorboat. In five lakes, one to three additional flux  
399 measurements were made amidst emergent macrophytes of different species (corresponding to  
400 the wet graminoid land cover class) short enough to fit into the flux chamber without excessive  
401 disturbance. The chamber comprised an inverted 25.4 cm tall, opaque white bucket with a 34.2  
402 cm diameter opening wrapped with a buoyant skirt made of foam tubing. An infrared greenhouse  
403 gas analyzer (EGM-4, PP Systems) was used to measure chamber air carbon dioxide (CO<sub>2</sub>)  
404 concentration and circulate chamber air via an inlet on the side of the chamber and an outlet in  
405 the center of its ceiling. A metal handle was used to steady the bucket for a 15-minute  
406 measurement period. At 0, 5, 10, and 15 minutes, gas samples were drawn from the chamber's  
407 headspace through the gas analyzer inlet tubing and injected into evacuated exetainers using a 30  
408 mL polypropylene syringe fitted with a 3-way stopcock for subsequent analyses of methane  
409 concentration.

410 The samples were analyzed on a Shimadzu GC-2014 gas chromatograph for methane  
411 partial pressure within two months of collection. Gas flux across the water-air interface was  
412 calculated from the rate of change in the chamber methane concentration over the deployment  
413 time and chamber area ( $\text{mol}\cdot\text{min}^{-1}\cdot\text{m}^{-2}$ ). The rates of change of methane concentrations in the  
414 chamber were generally linear with  $r^2$  values greater than 0.90. Given this linear response,  
415 ebullition was deemed negligible during the measurement periods. Thus, the closed, static  
416 chamber measurements included both diffusive fluxes from the water surface as well as any  
417 plant-mediated fluxes. For the three lakes where multiple emergent macrophyte fluxes were  
418 taken at one location, measurements from each water zone were averaged by lake. Finally, for  
419 sites where paired open water vs. littoral zone measurements were collected, we calculated the  
420 vegetated: open water flux ratio (hereafter: flux ratio) as the ratio between the average emergent  
421 macrophyte and open water measurements for each lake, where open water could include  
422 submerged macrophytes not detectable with UAVSAR.

423 During sampling, care was taken not to disturb the sediment, and if any bubbles were  
424 observed before or during the period, the measurement was aborted. Even so, three  
425 measurements were extremely high, implying sediment disturbance. To avoid potential bias,  
426 these measurements, which were greater than 2.2 standard deviations from the median, were  
427 discarded (the next-highest value was 0.17 standard deviations from the median). These three  
428 measurements all came from vegetated sites, so this data omission lessened the impact of  
429 emergent vegetation in our subsequent analyses.

430

### 431 2.3.7 Published flux chamber measurements

432 In addition to our own field measurements, we compiled a synthesis dataset of 58 paired  
433 flux measurements, with the aim of determining the flux ratio for each lake. Six of these

434 measurements corresponded to shallow (typically with a 2-4 m cutoff) versus deep regions of the  
435 lake, with no mention of adjacent macrophytes, and were only included for reference, while the  
436 remaining 52 were taken from vegetated versus open water fluxes, and were used for subsequent  
437 calculations. Each lake pair corresponded to one of 41 distinct lakes or lake regions during a  
438 single or multi-year-averaged sampling season, published in 21 papers (Kankaala et al. 2005;  
439 2013; Smith and Lewis 1992; Larmola et al. 2004; Huttunen et al. 2003; Juutinen et al. 2003;  
440 Villa et al. 2021; Burger et al. 2016; DelSontro et al. 2016; Bergström et al. 2007; Striegl and  
441 Michmerhuizen 1998; Ribaudo et al. 2012; Casper et al. 2000; Dove et al. 1999; Elder et al.,  
442 2022; Rey-Sanchez et al., 2018; Desrosiers et al., 2021; Engram et al. 2020; Natchimuthu et al.,  
443 2016; Wik et al., 2013, Jansen et al., 2020a; **Table S.3**). Lakes included boreal, tropical and  
444 temperate regions and were located in Finland, Quebec, Ontario, Alaska, Colorado, Ohio,  
445 Minnesota, Italy, the UK, and the Amazon and Orinoco river basins. For each paper, the  
446 average—whether seasonal or annual—vegetated and open water measurements were recorded  
447 and converted, if necessary, to units of  $\text{mg CH}_4/\text{m}^2/\text{day}$ . Four papers (Burger et al., 2016; Casper  
448 et al., 2000; Dove et al., 1999; Desrosiers et al., 2021) separately measured each of the three  
449 methane emission pathways, and most of the others focused on diffusion and/or plant-mediated  
450 fluxes. An additional six (Huttunen et al., 2003; Juutinen et al., 2003; Larmola et al., 2004;  
451 Striegl and Michmerhuizen, 1998; Jansen et al., 2020a; Villa et al., 2021) measured diffusion and  
452 ebullition in both lake zones, but did not place the flux chamber over plants, thus not accounting  
453 for that pathway. One study (Bergström et al., 2007) did not provide open water values, which  
454 we estimated based on lake area via the relationship of Holgerson and Raymond (2016). The  
455 dataset includes 55 diffusion, 40 plant-mediated, and 17 ebullition pairs, with some  
456 measurements counting towards multiple pathways.

457 The vegetated: open water flux ratio  $R$  was calculated for each applicable lake (including  
458 our field lakes) and divided by a correction factor of 1.33 to account for most measurements  
459 being made either during ice-covered or ice-free seasons, but not during ice melt, when open-  
460 water emissions can temporarily spike. The correction factor, averaged from Wik et al. (2016a)  
461 and Denfeld et al. (2018), comes from statements that 23% and 27% of emissions of ice-covered  
462 lakes, respectively, are attributed to ice-melt fluxes. Although the lake upscaling calculation by  
463 Rosentreter et al. (2021) also uses a spatiotemporal ice-cover correction with the opposite effect  
464 of the ice-melt pulse correction, we have omitted it here, assuming it affects both vegetated and  
465 unvegetated areas equally. The adjusted flux ratio  $R'$  therefore comes from measurements of  
466 three methane flux pathways, collected from both littoral vegetation and shallow open water in  
467 all seasons, and reflects adjustments to account for unmeasured ice-melt pulses.

468 Many papers stated the area covered by emergent macrophytes, but if not, Google Earth  
469 Pro and QGIS 3.10.11 were used to digitize, map project, and measure the approximate coverage  
470 area, with attention paid to the papers' description of the vegetation for context. Coverage areas  
471 were assigned an uncertainty value (typically 2–5%) based on interpretation of the methods used  
472 or confidence in our digitizing result. Although challenging to compare across methodologies,  
473 geographic regions, and plant types, this dataset served as a best estimate of flux ratios from a  
474 diverse global sample of lakes.

475

## 476 2.3.8 Sensitivity analysis

477 Likely ranges in whole-lake methane emissions were calculated using the following  
478 equation, mapped lake areas, and the compiled flux dataset:

$$479 \quad F_{total} = c * A_{LEV} * \Omega * R' * f_{OW} + (1 - c * A_{LEV} * \Omega) * f_{OW} \quad [1]$$

480 where  $F_{total}$  is the total lake flux (mg CH<sub>4</sub>/day), calculated as a weighted average of vegetated  
481 and open water zones;  $c$  is a scalar  $\leq 1$ , described in section 2.3.7, that corrects for potential  
482 double-counting of UAVSAR-observed emergent vegetation as wetlands contained in modeling  
483 datasets (unitless);  $A_{LEV}$  is the emergent vegetation area as a fraction of total lake area (unitless);  
484  $\Omega$  is the total lake area (m<sup>2</sup>),  $f_{OW}$  is the flux per area of open water (mg CH<sub>4</sub>/m<sup>2</sup>/day); and  $R'$  is  
485 the corrected ratio between emergent macrophyte and open water fluxes per area (unitless). All  
486 areas and fluxes are expressed relative to the total lake area  $\Omega$ , and the flux per unit area of open  
487 water ( $f_{OW}$ ), both of which cancel out when applying equations [1] and [2].

488 The impact of vegetation on whole-lake flux was calculated as a percent difference via:

$$489 \quad I = \frac{F_{total} - f_{OW} * \Omega}{f_{OW} * \Omega} \quad [2]$$

490 where  $I$  represents the percent increase from differentiating between open water and emergent  
491 vegetation within lakes.  $I$  is sensitive only to the measured parameters  $R'$ ,  $A_{LEV}$ , and  $c$ , and  
492 independent of the absolute magnitudes of the fluxes or areas attributed to each lake zone, which  
493 cancel out.

494 Equations [1] – [3] were applied using the median values of  $R'$  and  $f_{OW}$  and the lake area-  
495 weighted mean  $A_{LEV}$ . Median values were used due to the skewed distributions of  $R'$  and  $f_{OW}$ .  
496 The equations were also applied to the bootstrapped confidence intervals of  $A_{LEV}$  in order to  
497 estimate uncertainty.

498

499 **3 Results**

## 500 3.1 Inundation patterns at the landscape scale

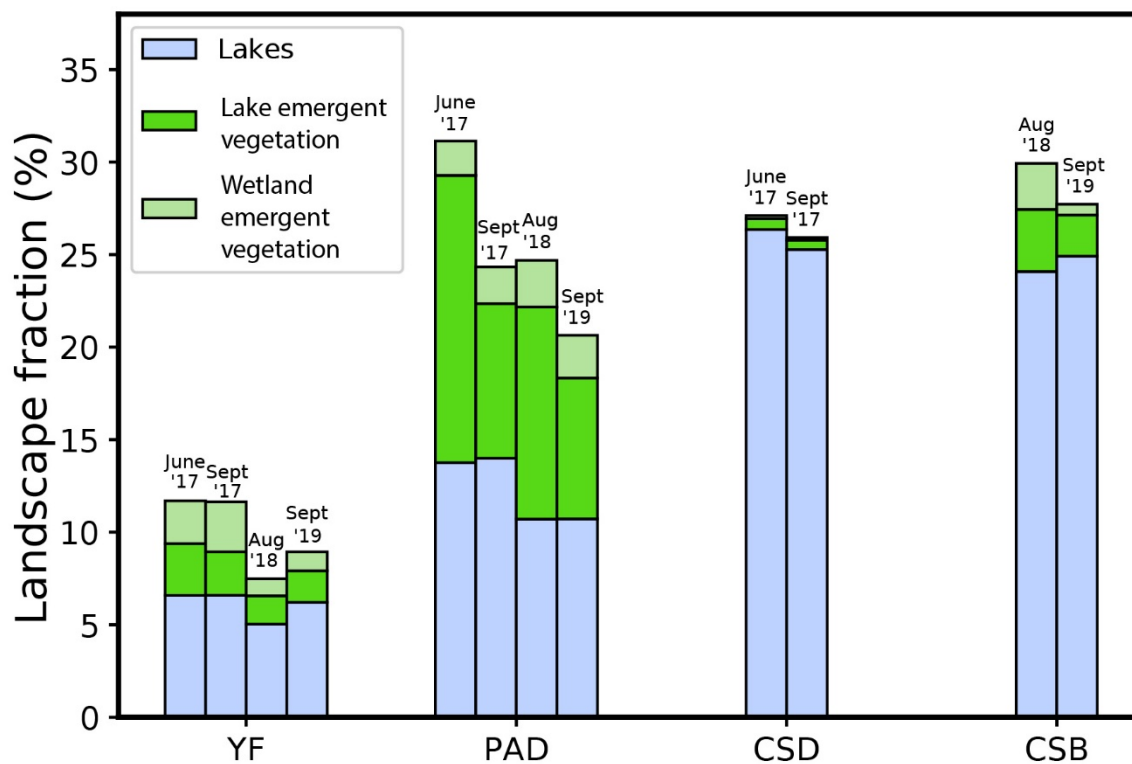
## 501 3.1.1 Regional and seasonal inundation characteristics

502 Significant open water, emergent vegetation, and wetland fractional areas are found in all  
503 study areas, vary seasonally as well as regionally, and are particularly extensive in the PAD and  
504 YF. The total area of the landscape covered by lake emergent vegetation (LEV) varies from 0.5 –  
505 0.6 % (CSD), 2.2 – 3.4 % (CSB), 7.6 – 15.5 % (PAD), and 1.7 – 2.8 % (YF) over the 2017-2019  
506 observational period (**Figure 2, Table 2**). In comparison, wetland emergent vegetation ( $A_{WEV}$ )  
507 covers  $\leq 2.7\%$  of the area in all sites (mean of 1.4%, **Table 2**). Most of the emergent vegetation  
508 is classified as either wet graminoid (WG, weighted mean of 69%) or shrub vegetation (WS,  
509 29%), with wet forest comprising  $<1\%$  of this area for all areas except YF, for which it covers a  
510 mean of 5.9%. When only considering LEV that falls within a global dataset lake (the double-  
511 counting correction), the graminoid fraction increases to 99.1% (GLOWABO) or 98.7%  
512 (HydroLakes), which provides further confidence that the remaining LEV is indeed littoral  
513 vegetation and not an adjacent, forested wetland, at least for large lakes in the global datasets.  
514 Virtually all detected emergent vegetation lies adjacent to shorelines, with  $< 0.2\%$  of their area

515 occurring completely within a lake with no connectivity to non-island land. These patterns show  
 516 that the dominant littoral vegetation type in the study areas is graminoids, which almost always  
 517 occur at the interface between land and water.

518 In all applicable study areas, total inundation (open water plus emergent vegetation) is  
 519 greater or equal in the early summer (June) than in late summer (August/September), likely due  
 520 to snowmelt. In the PAD, this change is caused by decreased LEV, with emergent wetland  
 521 vegetation remaining constant, implying that seasonal inundation changes occurred in flood-  
 522 tolerant eulittoral vegetation (**Figure 2, Table 2**). Thus, regional variations in emergent  
 523 vegetation, as well as open water, are greater than seasonal/interannual variations within study  
 524 areas.

525



526

527 **Figure 2.** Significant lake emergent vegetation (LEV) is found in all study areas, varies  
 528 seasonally as well as regionally, and is particularly extensive in the lowland PAD and YF. This  
 529 chart shows landscape fractional areas of open water and LEV classes for the Yukon Flats (YF),  
 530 Peace-Athabasca Delta (PAD), Canadian Shield – Daring Lake (CSD), and Canadian Shield –  
 531 Baker Creek (CSB), derived from airborne UAVSAR. LEV is defined as emergent vegetation

532 adjacent to open water, with remaining areas assigned to wetlands (WEV). Month and year of  
 533 UAVSAR flight acquisitions appear in text above each column.

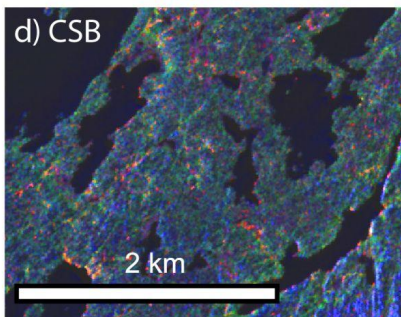
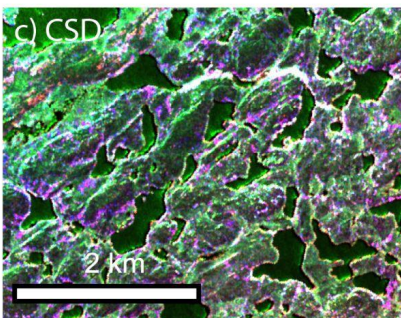
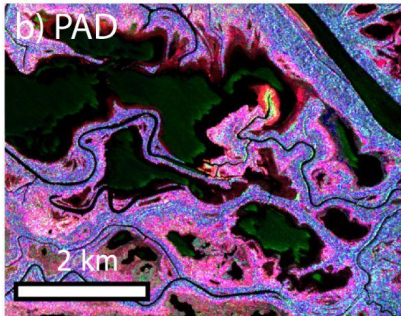
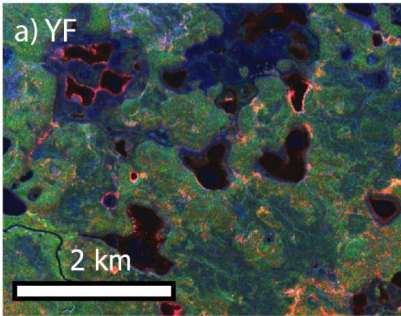
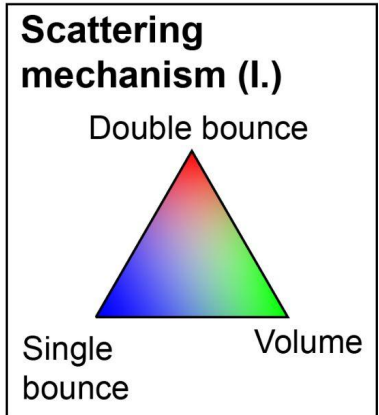
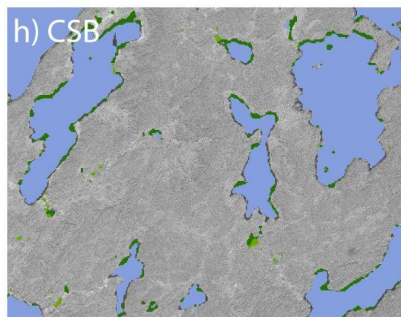
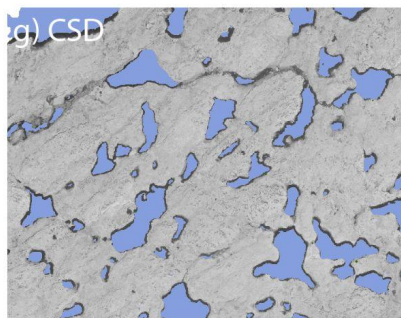
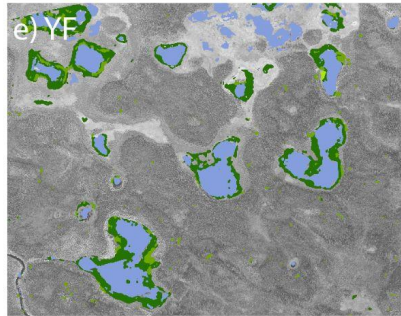
	Study area	Extent (km <sup>2</sup> )	Lake count	Lake fraction (%)				Landscape area (km <sup>2</sup> , %)							
				A <sub>LEV</sub>	A <sub>WF</sub>	A <sub>WS</sub>	A <sub>WG</sub>	A <sub>LEV</sub> (median)	A <sub>LEV</sub> (unweighted)	Lake open water	LEV	WF	WS	WG	WEV
CSD June 2017	CSD	3037	1918	1.1 [0.9, 1.4]	0.0 [0.0, 0.0]	0.0 [0.0, 0.1]	1.1 [0.9, 1.3]	0.0%	2.0%	800 (26.4%)	18 (0.6%)	0 (0.0%)	1 (0.0%)	17 (0.6%)	3 (0.1%)
CSD Sept 2017	CSD	3037	1975	0.9 [0.6, 1.1]	0.0 [0.0, 0.0]	0.0 [0.0, 0.0]	0.8 [0.6, 1.1]	0.0%	3.8%	767 (25.3%)	16 (0.5%)	0 (0.0%)	0 (0.0%)	15 (0.5%)	2 (0.1%)
CSB Aug 2018	CSB	3037	1947	1.0 [0.8, 1.2]	0.0 [0.0, 0.0]	0.0 [0.0, 0.1]	1.0 [0.7, 1.2]	0.0%	2.9%	784 (25.9%)	17 (0.5%)	0 (0.0%)	1 (0.0%)	16 (0.5%)	3 (0.1%)
CSB Sept 2019	CSB	1155	376	8.6 [5.8, 14.1]	0.0 [0.0, 0.1]	2.3 [1.7, 3.6]	6.2 [4.1, 10.5]	20.4%	26.6%	278 (24.1%)	39 (3.4%)	0 (0.0%)	11 (1.0%)	28 (2.4%)	29 (2.5%)
CSB	CSB	1160	378	5.5 [3.6, 9.0]	0.0 [0.0, 0.1]	0.7 [0.5, 1.1]	4.7 [3.1, 7.9]	11.3%	17.5%	289 (24.9%)	26 (2.2%)	0 (0.0%)	4 (0.3%)	22 (1.9%)	7 (0.6%)
CSB	CSB	1158	377	7.0 [4.7, 11.5]	0.0 [0.0, 0.1]	1.5 [1.1, 2.3]	5.5 [3.6, 9.2]	15.9%	22.1%	284 (24.5%)	32 (2.8%)	0 (0.0%)	7 (0.6%)	25 (2.1%)	18 (1.5%)
PAD June 2017	PAD	1339	347	65.5 [56.5, 75.3]	0.7 [0.2, 1.3]	35.3 [28.2, 42.6]	29.5 [21.4, 38.8]	63.5%	58.3%	184 (13.8%)	208 (15.5%)	2 (0.1%)	73 (5.4%)	133 (10.0%)	25 (1.8%)
PAD Sept 2017	PAD	1338	729	52.1 [42.8, 61.6]	0.1 [0.0, 0.3]	13.8 [9.0, 19.5]	38.2 [31.4, 45.3]	60.5%	56.2%	187 (14.0%)	112 (8.4%)	0 (0.0%)	18 (1.3%)	94 (7.0%)	26 (1.9%)
PAD Aug 2018	PAD	1338	366	61.4 [51.8, 70.8]	1.1 [0.3, 1.9]	39.3 [31.1, 47.6]	21.1 [15.8, 27.7]	68.4%	62.0%	143 (10.7%)	153 (11.4%)	1 (0.1%)	64 (4.8%)	88 (6.6%)	34 (2.5%)
PAD Sept 2019	PAD	1336	437	56.6 [49.2, 65.2]	0.3 [0.0, 0.6]	33.3 [26.9, 40.2]	22.9 [16.8, 31.1]	57.1%	57.7%	143 (10.7%)	102 (7.6%)	0 (0.0%)	42 (3.1%)	60 (4.5%)	31 (2.3%)
PAD	PAD	1338	470	58.9 [50.1, 68.2]	0.6 [0.1, 1.0]	30.4 [23.8, 37.5]	27.9 [21.3, 35.7]	62.4%	58.6%	164 (12.3%)	144 (10.7%)	1 (0.1%)	49 (3.7%)	94 (7.0%)	29 (2.1%)
YF June 2017	YF	2739	2687	24.9 [22.8, 27.2]	1.2 [0.2, 2.5]	4.0 [3.4, 4.8]	19.7 [18.0, 21.6]	31.8%	36.8%	180 (6.6%)	77 (2.8%)	4 (0.1%)	14 (0.5%)	58 (2.1%)	63 (2.3%)
YF Sept 2017	YF	2739	2857	22.6 [20.7, 24.7]	1.3 [0.3, 2.6]	5.5 [4.3, 6.8]	15.8 [14.6, 17.3]	27.0%	33.5%	180 (6.6%)	64 (2.3%)	4 (0.1%)	15 (0.6%)	45 (1.6%)	74 (2.7%)
YF Aug 2018	YF	2739	1784	22.4 [19.7, 25.3]	1.8 [0.3, 3.8]	4.6 [3.6, 6.0]	16.0 [14.3, 17.9]	17.0%	28.2%	138 (5.0%)	42 (1.5%)	3 (0.1%)	10 (0.4%)	30 (1.1%)	25 (0.9%)
YF Sept 2019	YF	2739	1533	18.5 [16.1, 21.2]	1.9 [0.4, 4.0]	2.3 [1.8, 3.0]	14.3 [12.7, 16.1]	15.6%	25.5%	170 (6.2%)	47 (1.7%)	3 (0.1%)	9 (0.3%)	35 (1.3%)	28 (1.0%)
YF	YF	2739	2215	22.1 [19.8, 24.6]	1.5 [0.3, 3.2]	4.1 [3.3, 5.2]	16.5 [14.9, 18.2]	22.8%	31.0%	167 (6.1%)	57 (2.1%)	3 (0.1%)	12 (0.4%)	42 (1.5%)	47 (1.7%)
Mean				22.3 [18.9, 26.4]	0.5 [0.1, 1.1]	9.0 [7.1, 11.3]	12.7 [10.1, 16.1]	25.3%	28.6%	350 (17.2%)	63 (4.0%)	1 (0.1%)	17 (1.2%)	44 (2.8%)	24 (1.4%)
Weighted mean				16.2 [13.9, 19.1]	0.5 [0.1, 1.1]	5.8 [4.5, 7.2]	10.0 [8.2, 12.2]	17.9%	21.8%	409 (16.9%)	53 (3.0%)	1 (0.1%)	13 (0.8%)	38 (2.1%)	24 (1.2%)
Mean (late summer)				21.4 [18.0, 25.6]	0.5 [0.1, 1.1]	8.6 [6.7, 10.9]	12.3 [9.8, 15.5]	24.4%	28.4%	343 (16.9%)	55 (3.6%)	1 (0.0%)	15 (1.0%)	39 (2.5%)	23 (1.3%)
Weighted mean (lt. s.)				15.0 [12.7, 17.8]	0.5 [0.1, 1.1]	5.3 [4.1, 6.7]	9.2 [7.5, 11.3]	16.4%	21.1%	401 (16.6%)	47 (2.7%)	1 (0.0%)	12 (0.7%)	34 (1.9%)	22 (1.1%)

535 **Table 2.** Within-lake emergent vegetation coverages ( $A_{LEV}$ ) by vegetation type ( $A_{WF}$  = area of  
536 wet forest,  $A_{WS}$  = area of wet shrub,  $A_{WG}$  = area of wet graminoid,  $A_{WEV}$  = area of wetland  
537 emergent vegetation, as opposed to lake vegetation) and by study area, along with landscape  
538 coverage in km<sup>2</sup> and as percent coverages. Numbers in brackets give the bootstrapped 95%  
539 confidence intervals. Weighted mean columns are weighted by individual lake area, and  
540 summary weighted mean rows are weighted by the total lake area of each study area for all dates  
541 and late summer only (August and September, abbreviated as lt. s. when necessary).

542

### 543 3.1.2 Validation of UAVSAR classifier

544 The land cover classifier successfully retrieves the three broad classes of emergent  
545 vegetation. Based on visual inspection of the land cover maps, the most significant  
546 misclassification is evidenced by false detections of water in areas actually covered by dry  
547 graminoid vegetation (**Figure 3e**, top middle) and false detections of inundated vegetation in  
548 areas of forest. The most frequent misclassification occurs between Wet Shrub and Rough  
549 Water, although errors of omission and commission are roughly equal, implying a near-zero net  
550 effect on the landscape totals (**Figure S.1**). Any misclassification among the dry land classes  
551 does not affect our lake analysis, and misclassification between the flooded and dry classes is  
552 rare, as expected, given the sensitivity of SAR to water presence (**Figure S.1**). Prior to the  
553 quality control measures (**Section 2.3.4**), Cohen's kappa coefficients are 0.862 for the model  
554 used on the simpler CSD landscape and 0.824 for the model used for the remaining sites,  
555 implying good agreement with the validation data. Since the analysis only uses flooded classes  
556 connected to open water that could be validated by optical imagery, errors of commission  
557 (**Figure S.1**) represent an upper bound.

**I. SAR Image****II. Classification**

558

559 **Figure 3.** Example L-band SAR images of subsets within the four study areas (**Column I. a-d**,  
 560 YF 6/2017, PAD 9/2019, CSD 9/2017, CSB 8/2018, respectively) and corresponding  
 561 classification (**Column II. e-h**). SAR images are colorized by Freeman-Durden scattering  
 562 mechanism (double bounce in red, primarily indicating emergent vegetation; volume scattering  
 563 in green, primarily indicating leafy vegetation; and single bounce scattering in blue, primarily  
 564 indicating bare ground, bedrock, and some types of trees) and are stretched identically, with  
 565 visual adjustments for brightness and color saturation. In column II., only inundated classes are

566 shown and are superimposed over a grayscale version of the color-infrared camera base map  
567 from Kyzivat et al. (2018), in which forests appear darker than grasslands or bedrock.

568

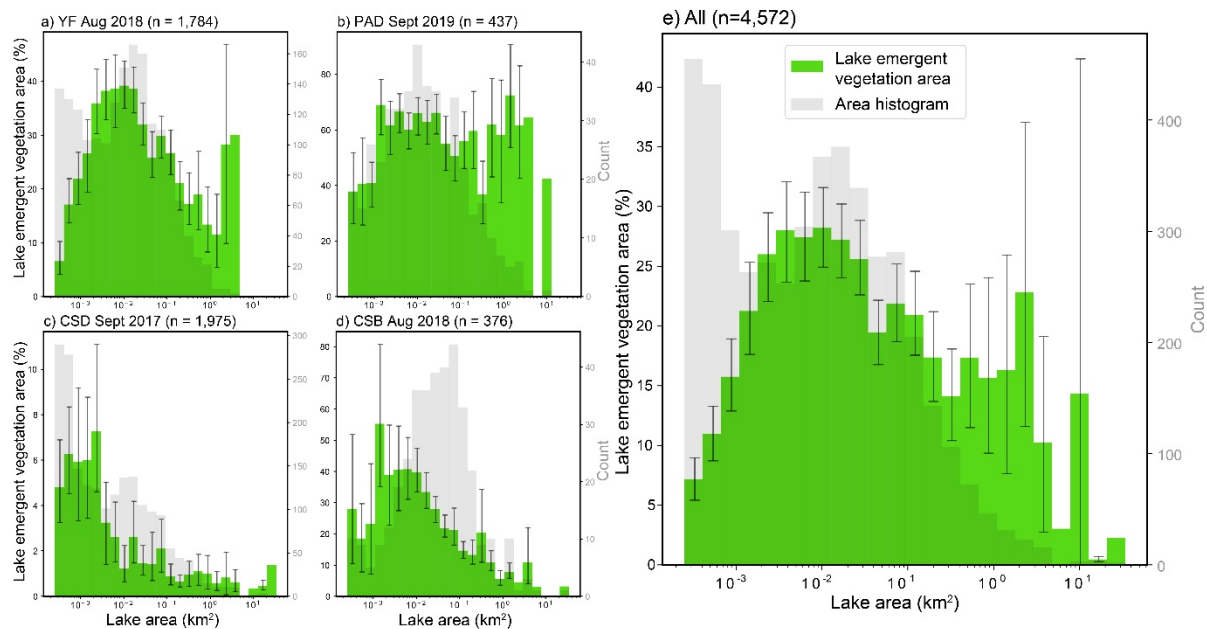
## 569 3.2 Emergent vegetation extent

### 570 3.2.1 Regional and morphological trends

571 Although useful for integrating all flux components, landscape-scale descriptors obscure  
572 the nuance of individual lake characteristics. Consequently, we also present results normalized  
573 by each lake's area and aggregated via weighted averaging (**Table 2, Figure 4**). With this  
574 normalization, it is more apparent that emergent vegetation ( $A_{LEV}$ ) is quite prevalent in lakes,  
575 averaging 16.2 [13.9 – 19.1]% across the four study areas, weighted by lake area. Again,  
576 coverage is especially extensive in the lowland PAD and YF (**Figure 2**), averaging 59 [50 –  
577 68]% and 22 [20 – 25]%, respectively.  $A_{LEV}$  in the more topographically constrained, colder,  
578 sparsely vegetated CSB and CSD areas averages 7.0 [4.7 – 11.5]% and 1.0 [0.8 – 1.2]%,  
579 respectively. The lowland sites, therefore, have the most  $A_{LEV}$ , both as a percentage of total lake  
580 area as well as landscape area.

581 While emergent vegetation is observed in every size bin in every area, we find only a  
582 weak relationship between  $A_{LEV}$  and lake area that holds for all study areas. The area bins  
583 comprising small to medium-sized lakes between 0.002 to 0.02 km<sup>2</sup> always contain the primary  
584 histogram peak, with the exception of the PAD, for which these bins contain the secondary peak  
585 (**Figure 4b**). In all regions except the PAD, the smallest observable lakes ( $\geq 250$  m<sup>2</sup>) have  
586 similar coverage to the largest ( $> 10$  km<sup>2</sup>), resulting in unimodal area-binned histograms, even  
587 within the confidence intervals (**Figure 4**). The drop in  $A_{LEV}$  for small lakes is likely caused by  
588 mixed pixels in narrow littoral zones being detected as water. Even so, Pearson correlation is  
589 weak between log-transformed  $A_{LEV}$  and lake area ( $r^2 = 0.124$ ,  $p < 0.001$ , **Figure 5**), implying  
590 that the inverse relationship between the two variables is not consistent across sites. On an  
591 individual basis, the two Canadian Shield study areas have significant regression relationships ( $p$   
592  $< 0.001$ , **Figure 5**), with  $r^2 = 0.25$  (CSB) and 0.48 (CSD), likely explained by their simpler,  
593 bedrock-dominated landscapes.

594

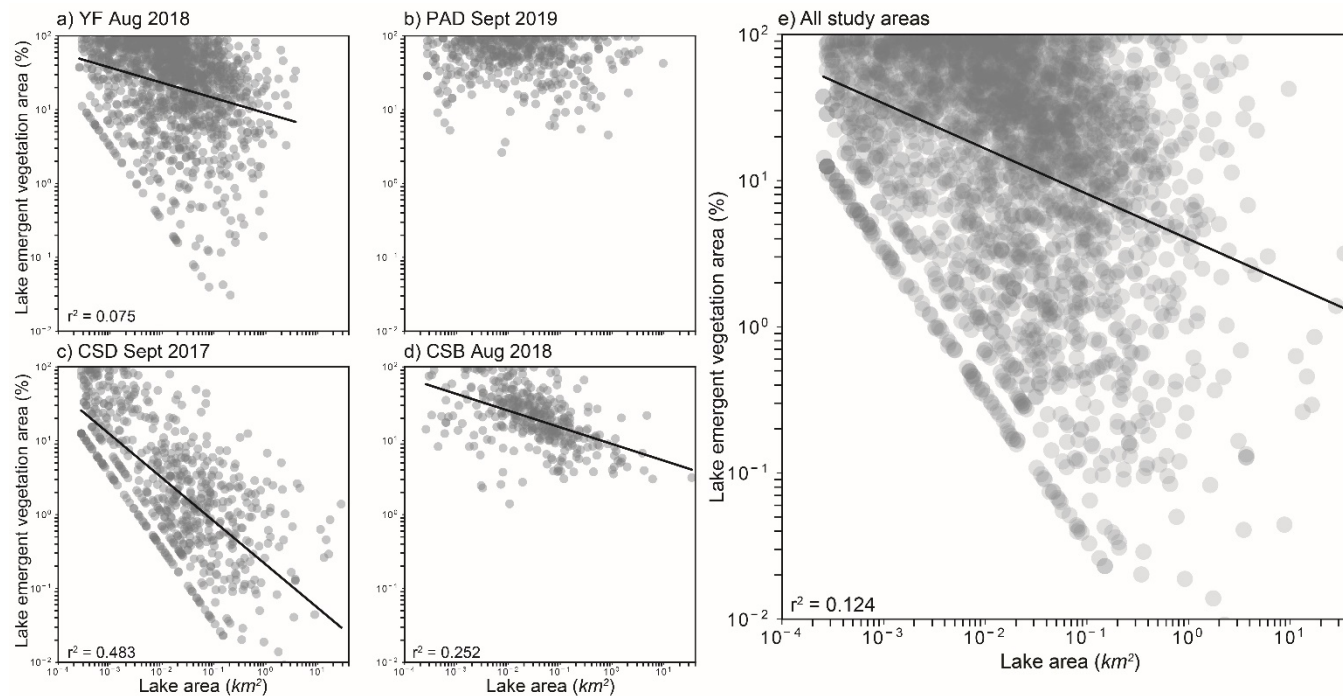


595

596 **Figure 4.** Emergent vegetation ( $A_{LEV}$ ) is most prevalent in small to medium-sized lakes. Here,  
 597 mean  $A_{LEV}$ , in green, is calculated for logarithmic lake area bins for each region (a) and for all  
 598 regions combined (b). Error bars give the 95% confidence interval for  $A_{LEV}$  for all bins with  $> 2$   
 599 observations. The lake count in each bin is plotted in grey and shows that most observed lakes  
 600 are much smaller than  $1 \text{ km}^2$ . Accordingly, bins with fewer lakes generally have greater  
 601 uncertainty in  $A_{LEV}$ , and the rightmost bins, which contain  $< 10$  lakes, have considerable  
 602 uncertainty. For a version of this figure showing bin sums, rather than means, see **Figure S.2**.

603

604



605  
 606 **Figure 5.** Scatter plot of lake area and emergent vegetation coverage ( $A_{LEV}$ ) for all 4,572 lakes by  
 607 study area (a-d) and aggregated (e). There is only a weak relationship between the two log-  
 608 transformed variables. The diagonal bottom-left boundary in most plots is caused by area  
 609 quantization by pixilation; since  $A_{LEV}$  is a fraction, the minimum possible  $A_{LEV}$  corresponding to a  
 610 one-pixel vegetated zone decreases as the denominator increases. Lakes with  $A_{LEV} = 0$  are not  
 611 shown nor included in the regression and regression lines are only included for  $p < 0.001$ .

### 612 3.2.2 Seasonal trends

613 Despite fluctuating water levels, the distribution of  $A_{LEV}$  across lakes of varying areas  
 614 remains largely similar across seasons and years (**Figure S.3**). In all study areas, there is a  
 615 histogram peak at lakes with little or no emergent vegetation (**Figure S.3 a-d**, leftmost bin), as  
 616 many areas lack the necessary conditions to support emergent macrophytes. The histogram drops  
 617 sharply with increasing  $A_{LEV}$  coverage: extremely quickly in the sparsely-vegetated CSD,  
 618 somewhat quickly in the more southern CSB, and gradually in YF. The negative-skewed PAD  
 619 distribution (tail on left) is an anomaly with high-coverage lakes common. Accordingly, the area-  
 620 weighted mean (58.9 %) is barely greater than the arithmetic mean coverage (58.6 %) in the  
 621 PAD, unlike the rest of the study areas and the aggregated total, for which these values can differ  
 622 by a factor of two (**Table 2**). There are also more lakes overall detected in the PAD during early  
 623 summer (**Figure S.3**), likely because temporarily submerged macrophytes would be detected as  
 624 open water and thus constitute lakes in our analysis. These effects are likely due to prevalence of  
 625 shallow open water wetlands, which are ubiquitous in the delta and are included in our lake  
 626 dataset as long as some area of open water ( $>$  one pixel, or  $\sim 30$  m<sup>2</sup>) is detected. Although there is  
 627 little seasonal variance to the  $A_{LEV}$  distribution, the corresponding methane fluxes may depend  
 628 greatly on plant activity, which varies between seasons. To avoid including seasonal wetlands as  
 629 lakes, we used only the late summer (low water season) land cover maps to calculate mean  $A_{LEV}$   
 630 and have broken down available flux data by season. The temporal invariance of the  $A_{LEV}$

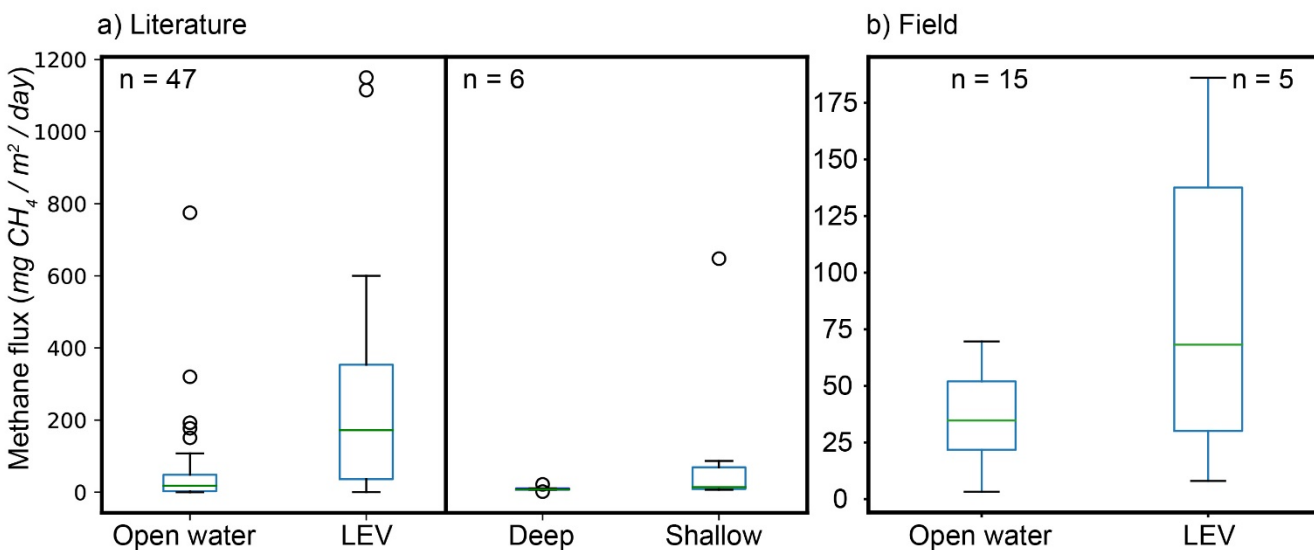
631 histograms provides further validation of the consistency of the classifier, and it shows how  
 632 changes in  $A_{LEV}$  are not relegated to the same small subset of lakes.

633

### 634 3.3 Methane fluxes from emergent macrophytes vs. open water

635 Field measurements confirm that methane fluxes per unit area from emergent  
 636 macrophytes are consistently higher than open water, even within the same lake (**Figure 6**).  
 637 Although macrophyte fluxes were only collected at five of the 15 visited PAD lakes, four have  
 638 higher mean macrophyte values than open water, leading to a mean macrophyte: open water flux  
 639 ratio of 2.3 (Kyzivat et al., 2021b). Given the small sample size, differences are not significant ( $u$   
 640  $= 2.0$ ,  $p = 0.19$ ,  $n = 5$ ) based on the non-parametric Mann-Whitney test. Strong variability in the  
 641 measurement may also contribute, since these short-term measurements exclude ebullition and  
 642 the other key episodic open water fluxes (ice-out flux, water column turnover fluxes) are  
 643 accounted for afterwards via a correction factor. Similarly, plants, as well as open water, can  
 644 have pronounced diel and seasonal variability in their fluxes, and these measurements were all  
 645 made during the day.

646 The fluxes obtained by literature synthesis (**Table S.3**) have an even more extreme  
 647 median ratio of 8.8 (**Figure 6**; **Figure 7**, top histogram), with a significant difference between  
 648 open water and vegetation ( $u = 1,800$ ,  $p < 0.001$ ,  $n = 47$ ). Of the 56 paired vegetation versus  
 649 open water measurements, all but eight have flux ratios  $> 1$ , implying greater emissions from  
 650 vegetated regions. The PAD and literature measurements combined have a median flux ratio of  
 651 6.1, or 15.9 if only Arctic-boreal lakes are included. We use the former, smaller value, since it  
 652 comes from a larger sample size, and multiply it by the ice-melt flux correction factor to obtain  
 653 4.6, which is used for the subsequent sensitivity calculation (**Table 3**). Due to limited data,  
 654 studies from all seasons and measurement periods were used, and some only measured one or  
 655 two of the emission pathways (see **2.3.6**). The four studies that defined lake zones based on  
 656 depth rather than vegetation yielded a median flux ratio of 15.8. Despite a limited and  
 657 spatiotemporally uneven global sampling, lakes in our study areas and worldwide unequivocally  
 658 trend towards higher emissions from emergent macrophyte environments than from open water.

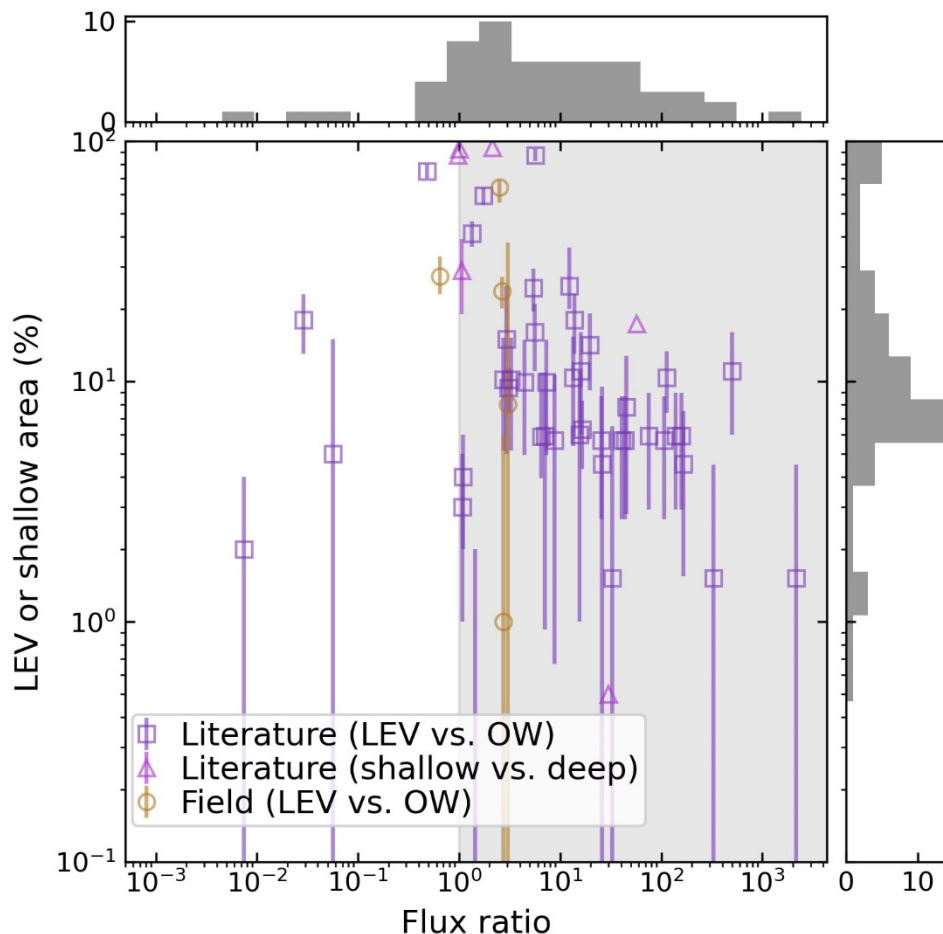


659

660 **Figure 6.** Lake emergent vegetation (LEV) and shallow regions produce greater methane fluxes  
661 than open water zones and deep regions, respectively, based on the literature (**a**) and from field  
662 measurements in the Peace-Athabasca Delta in July and August 2019 (**b**). Green lines show the  
663 median, hinges are drawn at the lower and upper quartiles, and flyer bars give the extent of data  
664 not considered outliers, which are plotted as points. Note the different scales demonstrating  
665 much greater flux values (mg of CH<sub>4</sub> /day) from the literature (**a**) than in the PAD (**b**).  
666

### 667 3.4 Sensitivity of whole-lake methane emissions to inclusion of vegetated areas

668 By applying the median corrected macrophyte: open water ratio of 4.6 (**Section 3.3**) to  
669 our remotely sensed UAVSAR LEV maps (**Figure 3**), we estimate the relative importance of  
670 accounting for emergent vegetation in whole-lake methane flux estimates (**Table 3**). Assuming a  
671 lake area weighted average  $A_{LEV}$  of 16.2 [13.9 - 19.1]% increases the overall methane emissions  
672 from the four study areas by 21 [18 - 25]% (**Figure 7**). Although the flux ratio  $R'$  has variability,  
673 we have not included it within the bounds of the estimate, relying instead on the more robust  
674 measurement of variance of  $A_{LEV}$ . Spatiotemporally, the impact ratio  $I$  varies from 4% to 321%,  
675 with the lower bound coming from CSD in September 2017 (where only ~0.9% of lake areas  
676 contains emergent vegetation) and the upper bound from the PAD in June 2017 (~66% coverage,  
677 **Table 2**). Although these are the most extreme values observed, these scenarios show that  
678 accounting for small, but numerous LEV zone areas significantly raises whole-lake emissions  
679 estimates.



680

681 **Figure 7.** Plotting study lakes in a flux ratio-emergent vegetation fraction feature space shows  
 682 that most emit more methane from lake emergent vegetation (LEV) than from open water on a  
 683 per-area basis (shaded region), leading to an overall median flux ratio of 6.1. Studies that  
 684 partitioned fluxes into shallow versus deep, rather than vegetated vs. open water zones  
 685 (triangular markers) are shown for reference but are not used for further analysis. The  
 686 distributions of both variables are shown as histograms along the relevant axes. Vertical error  
 687 bars show the temporal range in coverage for the field data (orange circles) and the estimated  
 688 mapping uncertainty for the literature data (purple squares) and can extend to zero (beyond axis  
 689 limits). For scale, the uppermost square data point in the figure (peat pond, Ontario, Canada,  
 690  $A_{LEV} = 88\%$ ,  $R=5.7$ ) corresponds to a 113% increase in emissions compared to the no LEV zone

691 case. Note the logarithmically-scaled x and y axes. For a version of this figure with contour lines  
 692 for the impact  $I$ , see **Figure S.4.4**.

693

$A_{LEV}$	$c$	$R$	$R'$	$I$
16.2 [13.9 – 19.1]%	0.36	6.1	4.6	21 [18-25]%

694 **Table 3.** Parameters and results of sensitivity calculation (**Equations 2 and 3**).  $A_{LEV}$  is area, with  
 695 95% confidence intervals, of lake emergent vegetation and is corrected for double-counting with  
 696 wetlands by the scalar  $c$ .  $R$  is the median global vegetated: open water flux ratio obtained from  
 697 the literature and is adjusted to  $R'$  correct for unmeasured ice-melt fluxes. The summary statistic  
 698  $I$  represent the impacts of accounting for LEV in whole-lake methane flux estimates.

## 699 4 Discussion and Conclusion

### 700 4.1 Emergent vegetation coverage in lakes

701 Littoral zones are often theorized to cover greater portions of small lakes than of large  
 702 lakes (Bergström et al., 2007; Wetzel, 1990, 2001). It is logical that smaller lakes with larger  
 703 perimeter: area ratios would be dominated by near-shore areas, which are overwhelmingly  
 704 shallow. However, while our results generally show greater fractional emergent vegetation area  
 705 ( $A_{LEV}$ ) in small and medium-sized lakes (**Figure 4**), there is weak correlation at best (Pearson  $r^2 =$   
 706 0.124,  $p < 0.001$ ; **Figure 5**). This discrepancy can likely be explained by lake emergent  
 707 vegetation (LEV) comprising only a portion of the littoral zone, as well as mixed pixels  
 708 obscuring narrow littoral margins in small lakes. Bergström et al. (2007) similarly observed that  
 709 medium-sized lakes (0.1 to 1 km<sup>2</sup>) had the greatest  $A_{LEV}$  of ~11% on average for 50  
 710 Fennoscandian Shield lakes in Finland, which, plotted as an area-binned histogram, also  
 711 resembles an inverted V-shaped curve. Mäkelä et al (2004), using the same dataset, pointed out  
 712 that large, lowland lakes had the largest total macrophyte coverage, also noting that area and pH  
 713 only account for 15% variation in  $A_{LEV}$ .

714 In comparison, the Canadian Shield areas we sampled contained the greatest  $A_{LEV}$  in  
 715 small-to-medium lakes (0.0001 - 0.002 km<sup>2</sup> in area), with values ranging from 7.3 [4.5 – 10.7] %  
 716 (CSD) to 55 [35 – 81] % (CSB). We also observe a large contribution to total  $A_{LEV}$  from the large  
 717 lakes (**Figure S.2**), underscoring the need not to discount them. Incidentally, these lakes are  
 718 under-represented in lake methane datasets (Deemer & Holgerson, 2021). The largest 100 lakes  
 719 (area  $\geq 0.9$  km<sup>2</sup>) comprise 62.7% of total lake area and 39.2% of total LEV area across all four  
 720 study areas, and this trend holds across all study areas (**Fig S.2**). The observed region-specific  
 721 dependence on lake area further highlights the need for remote sensing to estimate littoral or  
 722 vegetated zone coverage as well as to identify the interface between wetlands and open waters in  
 723 the context of aggregated methane emission estimates.

724 The ~16% mean  $A_{LEV}$  coverage we observe is greater than the globally-inclusive estimate  
 725 of 7% (Duarte et al., 1986) and Southern Finland estimate of 5.2% (Bergström et al., 2007). Since  
 726 the number is an intermediate average derived from much lower values on the Canadian Shield  
 727 (1.0%, and 7.0% for CSD and CSB, respectively, **Table 2**) and much higher values for the PAD

728 (59%) and YF (22%), it is highly sensitive to the choice of study areas and their relative sizes.  
729 Even though the relationship between coverage and lake area does not appear as simple as  
730 suggested by Duarte et al. (1986), their conclusion that lake area is not a strong predictor of  
731 emergent macrophyte coverage is still supported. Although the Boreal–Arctic Wetland and Lake  
732 Dataset (BAWLD; Olefeldt et al., 2021a; Olefeldt et al., 2021b) does not explicitly map littoral  
733 vegetation, the authors defined all open-water ecosystems as lakes, which includes shallow open-  
734 water wetlands. As a result, their lake class is defined nearly identically to ours, and they cite  
735 similar reasons regarding the importance emergent macrophytes as controls on net emissions.  
736 Indeed, comparison between datasets shows similar (ranging from 3-46% difference) lake  
737 coverage in each study area and an identical area-weighted mean over all study areas (16.6%,  
738 **Table S.6**). The roughly equivalent emergent vegetation and/or wetland classes are 24% greater  
739 in BAWLD (3.8% areal coverage from UAVSAR, 4.7% from BAWLD), which indicates that  
740 some or all LEV is included within BAWLD wetlands. BAWLD therefore represents best  
741 practices not only in ensuring a consistent lake-wetland distinction, but also presumably in  
742 including lake emergent vegetation within a wetland class, where it can be assigned a more  
743 appropriate methane flux.

## 744 4.2 Importance of emergent vegetation for methane upscaling

### 745 4.2.1 Toward improved upscaling of lake methane emissions

746 This broad-domain study supports previous studies demonstrating the importance of  
747 accounting for vegetated and/or littoral areas in upscaling lake methane flux estimates  
748 (Bergström et al., 2007; Casas-Ruiz et al., 2021; DelSontro et al., 2018a; Juutinen et al., 2003;  
749 Kankaala et al., 2013; Natchimuthu et al., 2016; Smith & Lewis, 1992; Striegl &  
750 Michmerhuizen, 1998). However, in addition to the challenges of measuring wetland extent  
751 more generally (Melton et al., 2013), a knowledge gap remains about the distribution and area of  
752 lake littoral zones (Huttunen et al., 2003). Our airborne UAVSAR approach for detecting LEV  
753 has limited spatial coverage and is unsuitable for broader-scale studies. Satellite approaches,  
754 however, have good utility for pan-Arctic or global wetland mapping (Hess et al. 1990, Nelson et  
755 al. 2006, Ghirardi et al. 2019, Zhang et al. 2021) and are well suited for study of large lakes,  
756 which contribute most to total LEV area (**Fig S.2**). These lakes are otherwise considered low  
757 methane emitters on a per-area basis (Holgerson & Raymond, 2016) and have little risk of being  
758 double-counted in wetland datasets, so they would be a good starting point for future studies.  
759 Incidentally, DelSontro et al. [2018] define an underestimation ratio between pelagic and littoral  
760 methane concentrations (roughly the inverse of  $I$ ) and show that it approaches unity for larger  
761 lakes, although they do not calculate the impact of these lakes to total lake emissions. The  
762 upcoming NISAR satellite mission is likely to provide high-resolution, freely available global  
763 coverage of L-band SAR, which may facilitate similar analysis for  $A_{LEV}$  over larger scales.

764 Unfortunately, our results do not reconcile the gap between modeled methane fluxes from  
765 bottom-up and top-down models (Thornton et al. 2016; Saunois et al., 2020). In fact, they  
766 suggest bottom-up fluxes are slightly greater than previously thought, which further widens the  
767 discrepancy. The most recent aquatic upscaling studies (Saunois et al., 2020; Rosentreter et al.,  
768 2021) and a recent wetland synthesis dataset for modeling (Zhang et al., 2021) used a consistent  
769 lake mask when defining lake and wetland areas, and this careful lake masking has not  
770 significantly improved the discrepancy (Saunois et al., 2020). These masks either come from  
771 global lake datasets (HydroLakes, GLWD, GLOWABO), or the more recent global surface water

772 explorer (GSW). Both GLOWABO and GSW were derived from 30 m resolution, optical  
773 Landsat satellite data, which is quite effective at detecting open water. It is unclear whether these  
774 methodologies include vegetation as part of lakes, although GLOWABO and HydroLakes show  
775 good agreement with our open water class (**Table S.4**). Wetland detection is more challenging  
776 and hampered by scale disparities between the relevant satellite sensors and inconsistent wetland  
777 definitions between disciplines ([Poulter et al., 2017]; Zhang et al., 2021). Thus, the practice of  
778 using consistent open-water lake masks to differentiate between lakes and wetlands is a good  
779 one.

780 Our results show that even after correcting for double-counted wetlands, UAVSAR  
781 detects emergent vegetation in 5.8% of lakes contained in global datasets. Whether through  
782 temporal change or dissimilar mapping methods, this discrepancy is large enough to have an  
783 impact on estimates of the lake contribution to the global methane budget. Equally important, but  
784 not demonstrated here, is accounting for the uniquely high emissions from non-vegetated lake  
785 littoral zones, which are less likely to be confused with wetlands, and are probably at least as  
786 extensive as LEV (Seekell et al., 2021). Non-vegetated littoral zones can also be high emitters,  
787 especially when within the reach of carbon-exuding roots and rhizomes (Bansal et al. 2020).  
788 Since mapped LEV falls within littoral zones by definition, it shares some of their properties, but  
789 our analysis does not attempt to separate these drivers. Even so, Jansen et al. (2020a) found no  
790 clear depth difference in the diffusive fluxes from two lakes in Stordalen Mire, Sweden, despite  
791 maximum depths of 5 and 7 m and a robust sampling strategy. However, ebullitive emissions  
792 from these same lakes showed a clear depth gradient (Wik et al. 2013). Our compiled synthesis  
793 data on depth, while limited, also shows no significant difference between deep and shallow  
794 emissions (Mann Whitney test,  $u = 10$ ,  $p = 0.24$ ,  $n = 6$ ), highlighting the need for more reporting  
795 of fluxes from different pathways and depth zones.

796 Given that our LEV flux data includes all emission pathways in a variety of lake types,  
797 the derived flux ratios represent a combination of many correlated drivers, including  
798 shallowness, methane oxidation, variable inundation, proximity to terrestrial inputs, and  
799 microbial community. In the context of deriving spatially explicit representations of methane  
800 emissions, it could be preferable to move away from using discrete land cover classes, and  
801 develop continuous representations of the processes that control methane production and rates of  
802 flux. These representations could better describe gradually-varying conditions, such as water  
803 table depth, the resulting concentration of oxygen in the subsurface, and the inclusion of new  
804 estimates of soil moisture, and they could improve estimates of methane emissions along  
805 hydrologic gradients.

806

#### 807 4.2.2 Limitations and future directions

808 Our 21% estimate for  $I$  (**Equation 2**), the percent increase due to including emergent  
809 vegetation in lake methane flux accounting, uses assumptions chosen to lead to the smallest  
810 possible value. Regardless, it is highly sensitive to the data-limited input parameters  $c$  and the  
811 flux ratio, which has a large variability that we have not accounted for. The double-counting  
812 correction factor  $c$  may suffer from lack of generality, since it was calculated only within the  
813 boundaries of our study regions using global datasets collected  $\sim 20$  years prior. It also assumes  
814 that LEV zones have similar areal emission to wetlands, which may not be valid. Clearly, more  
815 methane flux measurements in shallow or vegetated zones and estimates of total macrophyte

816 coverage are needed (Bergström et al., 2007; Schmiedeskamp et al., 2021). While our approach  
817 for correcting for double counting is only based on lakes large enough to be included in global  
818 datasets, the small magnitude of  $c$  shows how easy it is to count wetlands as LEV. Without this  
819 correction factor,  $I$  would be more than doubled to 58%. Future work should look more  
820 generally at the cause and magnitude of lake/wetland double counting (Thornton et al., 2016) and  
821 develop continuous metrics for methane emission habitats that don't rely on discrete land cover  
822 classes.

823 Our estimate for  $I$  may still be too high because our  $A_{LEV}$  includes up to 2.6% emergent  
824 shrubs and trees, even after the double-counting correction (**Table S.5**). This woody vegetation  
825 lacks the aerenchyma tissue that allows most wetland plants to transport methane from the  
826 sediments. Recent work has shown the potential for microbes living inside trees to produce  
827 methane (Covey & Megonigal, 2019), although this effect is likely less than soil microbe  
828 production. Secondly, the relatively narrow swath width of UAVSAR causes large (and likely  
829 less-vegetated) lakes to be under-represented in the calculation of weighted mean  $A_{LEV}$ . Adding  
830 to this effect is the use of the same vegetated: open water flux ratio for lakes of all sizes, when  
831 smaller lakes and ponds are known to be higher open-water methane emitters than large  
832 (Michmerhuizen, Striegl, & McDonald, 1996; Bastviken et al., 2004; Holgerson & Raymond,  
833 2016; Engram et al. 2020), probably because littoral zones (vegetated and unvegetated) cover  
834 most of their areas. Indeed, Kankaala et al. (2013) showed that the flux ratio increases with lake  
835 size. It follows that our concept of a vegetated: open water flux ratio is less useful for small lakes  
836 and would likely be even larger for the largest lakes, which were under-represented in our  
837 literature synthesis. Future studies could better quantify how this ratio varies based on lake area.  
838 Nevertheless, since the contribution to total  $A_{LEV}$  from the small lakes is so slight (**Fig S.2**), they  
839 don't have a large negative impact on our estimate. Finally, the estimate compares to a  
840 hypothetical upscaling using solely open water fluxes, while in reality, some studies include  
841 open-water measurements from entire littoral zones. While many of the studies cited here used  
842 area-weighted approaches with regard to lake depth zones (Natchimuthu et al., 2016; DelSontro  
843 et al, 2016; Jansen et al. 2020a), they appear to be a minority and are not available on the global  
844 scale (Kuhn et al. 2021b; Wik et al. 2016b).

845 Comparison of our sensitivity study with previous Arctic-boreal and global lake studies  
846 suggests that our finding of a 21% increase in whole-lake methane flux is conservative. Using  
847 flux chamber measurements from two Swedish lakes, Natchimuthu et al. (2016) found that  
848 methane emissions from lake centers are 2.1 times less than whole-lake fluxes, although fluxes  
849 were not explicitly measured near lake macrophytes. Similarly, Kankaala et al. (2013) found that  
850 74-82% of diffusive and plant-mediated emissions in 12 Finnish lakes derived from littoral  
851 macrophyte stands comprising only 5% of their total area. These amounts correspond to a flux  
852 ratio of 54-86, leading to an impact,  $I$ , on whole-lake fluxes between 270 and 430% greater than  
853 a case where open water fluxes were assumed throughout. Most recently, Desrosiers et al. (2022)  
854 found that the 26% of a boreal lake covered in macrophytes was responsible for 81% of its  
855 carbon emissions. The impact of considering the *Typha latifolia* stands alone can be calculated at  
856 102%. Although focused only on extremely high-emitting lake and wetland thermokarst hot  
857 spots, Elder et al. (2021) conducted a study of remotely-sensed methane "hot spot" emissions  
858 across a 70,000 km<sup>2</sup> Arctic-boreal domain and found an even greater disproportionality, where  
859 0.005% of the domain was estimated to emit 0.3-16.2 % of the total. The higher reported flux  
860 ratios from lake studies can be partly attributed to area-weighted analyses including much larger,  
861 and thus lower-emitting per unit area, lakes than our airborne-based study. Yet, they also

862 underscore the pitfalls of assigning higher areal fluxes to vegetated lake zones without ensuring  
863 these zones are not otherwise counted as wetlands.

864 Even when using best practices to avoid double-counting lakes with wetlands, the coarse  
865 resolution of global lake maps can still cause uncertainty in the precise location of shorelines. At  
866 the medium resolution of Landsat (30 m), the entire littoral zone could be “hidden” inside of  
867 mixed pixels at lake boundaries, even for large lakes, if they have steep margins. If only unmixed  
868 pixels are classified as lakes, it is unclear how near-shore land pixels would be treated, especially  
869 given that global wetland maps are typically made from coarser-resolution sensors (Zhang et al.,  
870 2021). Unfortunately, this hard-to-resolve small strip of land/water interface is precisely the area  
871 with the greatest impact on full-lake (DelSontro et al. 2018, Thornton et al. 2016) and landscape  
872 (Elder et al. 2021) fluxes, so it cannot be rounded off. Furthermore, due to changing inundation  
873 and vegetation coverage, lakes can contain LEV even if attempts are made to exclude it, such as  
874 from static lake maps. Littoral zones often have fluctuating inundation, and there are valid  
875 reasons to count them as either lakes or wetlands, even though current upscaling efforts require  
876 making this distinction. Just as with wetlands, lakes can be defined differently across disciplines.  
877 Although plant-mediated emissions are often reported in studies focused on lakes, upscaling  
878 studies frequently exclude vegetated areas from their lake estimates (Bastviken et al., 2011; Wik  
879 et al., 2013; Olefeldt et al., 2021a; Rosentreter et al., 2021), a best practice to avoid double-  
880 counting. This exclusion requires careful treatment of the fluxes from which “lake” estimates  
881 should be derived. Future work should develop techniques that can more accurately measure  
882 littoral zone area (Seekell et al., 2021), produce consistent and methane-relevant lake versus  
883 wetland criteria from remote sensing (Olefeldt et al., 2021a), and make use of temporally-  
884 dynamic inundation maps (Pekel et al., 2016; Zhang et al., 2021) for both wetlands and lakes.

885 Finally, since ebullition is under-represented in the synthesis dataset and not present in  
886 the field dataset, there may be biases present due to its episodic temporal pattern. We would  
887 expect a positive bias to  $R$ , since there is evidence that both diffusion and porewater  $\text{CH}_4$   
888 concentrations are reduced when there is an available plant pathway (Bansal et al. 2020). If this  
889 trend holds for ebullition as well, then ebullition would be greater in non-vegetated zones. Even  
890 so, of the 10 flux ratios that include ebullition among the measured pathways and use zones  
891 based on vegetation presence/absence, the median ratio is 6.5 (**Table S.3**), which hardly differs  
892 from the full dataset median of 6.1 (unpaired Mann-Whitney  $u = 1,600$ ;  $p = 0.052$ ,  $n = 13$  and  
893 39). Similarly, the use of a correction factor to compensate for missing ice-out flux  
894 measurements may too presumptive. Jammet et al. (2015) measured large spring fluxes in a very  
895 shallow peatland lake (<2 m), which suggests that methane accumulates in the sediments as well  
896 as in the water column over winter, and both shallow and deep areas would contribute to the  
897 spring efflux of  $\text{CH}_4$ . Further research is necessary to investigate how the flux ratio might change  
898 based on seasonality and pathway. In the absence of robust flux ratio data collected separately  
899 for each pathway, we do not attempt to correct for under-reported ebullition measurements.

900 Estimating Arctic-boreal lake methane emissions is constrained by limited data and  
901 reliance on assumptions such as discrete land cover classes. As noted by Saunio et al. (2020),  
902 methane upscaling can be improved by considering spatiotemporal variability and increasing  
903 sampling efforts in lakes with diverse morphologies and environmental conditions. Previous  
904 estimates have calculated a high bias caused by most measurements being made during waking  
905 hours (Sieczko et al., 2020) or summertime sampling (Wik et al., 2016a; Denfeld et al., 2018;  
906 Jansen et al., 2020b); or from static inundation maps (Hondula et al., 2021). Others have shown

907 low biases from insufficient seasonal (Wik et al., 2016b), or spatial (Wik et al., 2016b;  
908 Natchimuthu et al., 2016; Desrosiers et al., 2021) sampling. This study also suggests a low bias  
909 from not separately accounting for LEV, on par with the contribution of under-sampled ice melt  
910 flux, which ranges from 23 to 27%. Even so, inadequate and geographically-uneven sampling of  
911 the world's > 117 million lakes (Verpoorter et al., 2014) is likely the greatest source of  
912 uncertainty in lake upscaling. In the absence of sufficient data, upscaling estimates should make  
913 use of available quantitative corrections and continue to find and remediate sampling biases.

#### 914 4.3 Conclusion

915 Lake emergent vegetation (LEV) is ubiquitous in Northern lakes but limited data prohibit  
916 its inclusion in upscaling lake methane emissions. We provide a first assessment of its  
917 prevalence across 4,572 lakes in four Arctic-boreal regions using airborne UAVSAR mapping  
918 and find that they cover 16.2 [13.9 – 19.1]% of Arctic-boreal lakes on average, a higher amount  
919 than other estimates, but with strong differences between study areas. LEV is greatest in lowland  
920 riverine areas, where changing water levels cause seasonal variability. Consistent with previous  
921 studies, we find that it is more common in small than large lakes, but this relationship is weak  
922 and varies regionally. Accounting for LEV, using a synthesis of paired open water and LEV field  
923 measurements of methane flux, leads to an upscaling estimate 21 [18 - 25]% greater than an  
924 estimate that assigns the same open water flux to the entire lake. We conclude that multi-  
925 temporal remote sensing of littoral zones, based on vegetation or otherwise, and collection of  
926 flux data from all parts of a lake are necessary for accurate upscaling of lake methane emissions.  
927 Future studies should continue using consistent definitions to separate lakes and wetlands,  
928 incorporate temporal wetland and lake change into analyses, remain vigilant against double  
929 counting with wetlands, and use multiple lake zones or continuous metrics for upscaling.

930

#### 931 **Acknowledgments**

932 We thank Robert and Barbara Grandjambe for guiding services; Queenie Gray and Wood  
933 Buffalo National Park for enabling our field visits; Alex Shapiro of Alaska Land Exploration  
934 LLC for helicopter piloting; the U.S. Fish and Wildlife Service, the Gwichyaa Zhee Gwich'in  
935 Tribal Government and Doyon Limited for access to Yukon Flats National Wildlife Refuge;  
936 Michael W. Denbina for assistance with UAVSAR data processing; and Kevin Timoney for  
937 assistance with botanical identifications. Field work was conducted on or near land belonging to  
938 the Athabasca-Chipewyan, Mikisew Cree, Métis, and Gwich'in indigenous peoples. Resources  
939 supporting this work were provided by the NASA High-End Computing (HEC) Program through  
940 the NASA Center for Climate Simulation (NCCS) at Goddard Space Flight Center via the  
941 ABoVE Science Cloud. UAV Orthomosaics were created using DroneDeploy software. Data  
942 processing was made possible in part by the free and open-source software, including python,  
943 numpy, pandas, as well as with PolSAR Pro v5.1, which is provided by the European Space  
944 Agency (ESA). Any use of trade, firm, or product names is for descriptive purposes only and  
945 does not imply endorsement by the U.S. Government. Thanks to Lawrence Vulis and two  
946 anonymous reviewers who have greatly improved the manuscript.

947 **Funding**

948 This work was funded by the following NASA programs; Future Investigators  
 949 in NASA Earth and Space Science and Technology (FINESST), grant number  
 950 80NSSC19K1361, managed by Dr. Allison Leidner; Terrestrial Ecology Program Arctic-Boreal  
 951 Vulnerability Experiment (ABoVE), grant number 80NSSC19M0104, managed by Dr. Hank  
 952 Margolis; and the NASA Surface Water and Ocean Topography mission, grant number  
 953 NNX16AH83G, managed by Dr. Nadya Vinogradova Shiffer. US Geological Survey (USGS)  
 954 LandCarbon Program provided funding for KPW, RGS, MMD, and FGT.

955 **Data and software availability**

956 UAVSAR data used for this study can be downloaded at [https://uavsar.jpl.nasa.gov/cgi-](https://uavsar.jpl.nasa.gov/cgi-bin/data.pl)  
 957 [bin/data.pl](https://uavsar.jpl.nasa.gov/cgi-bin/data.pl). The derivative land cover maps and lake emergent vegetation shapefiles can be  
 958 found at the accompanying data publication: <https://doi.org/10.3334/ORNLDAAAC/1883>.  
 959 Methane flux data from the PAD can be found at  
 960 <https://doi.org/10.6073/pasta/1e0cadadd8024c8fabc692ee21dc1f57>. All MATLAB, Python and  
 961 shell scripts used in data processing can be found at <https://doi.org/10.5281/zenodo.5974901> and  
 962 <https://doi.org/10.5281/zenodo.5974915>.

963 **References**

- 964 Ayoub, F., Jones, C. E., Lamb, M. P., Holt, B., Shaw, J. B., Mohrig, D., & Wagner, W. (2018).  
 965 Inferring surface currents within submerged, vegetated deltaic islands and wetlands from  
 966 multi-pass airborne SAR. *Remote Sensing of Environment*, 212, 148–160.  
 967 <https://doi.org/10.1016/j.rse.2018.04.035>
- 968 Bansal, S., Johnson, O. F., Meier, J., & Zhu, X. (2020). Vegetation Affects Timing and Location  
 969 of Wetland Methane Emissions. *Journal of Geophysical Research: Biogeosciences*, 125(9),  
 970 e2020JG005777. <https://doi.org/10.1029/2020JG005777>
- 971 Bastviken, D., Cole, J., Pace, M., & Tranvik, L. (2004). Methane emissions from lakes:  
 972 Dependence of lake characteristics, two regional assessments, and a global estimate. *Global*  
 973 *Biogeochemical Cycles*, 18(4), 1–12. <https://doi.org/10.1029/2004GB002238>
- 974 Bastviken, D., Tranvik, L. J., Downing, J. A., Crill, P. M., & Enrich-Prast, A. (2011). Freshwater  
 975 Methane Emissions Offset the Continental Carbon Sink. *Science*, 331(6013), 50–50.  
 976 <https://doi.org/10.1126/SCIENCE.1196808>
- 977 Bergström, I., Mäkelä, S., Kankaala, P., & Kortelainen, P. (2007). Methane efflux from littoral  
 978 vegetation stands of southern boreal lakes: An upscaled regional estimate. *Atmospheric*  
 979 *Environment*, 41, 339–351. <https://doi.org/10.1016/J.ATMOSENV.2006.08.014>
- 980 Bourgeau-Chavez, L. L., Endres, S., Powell, R., Battaglia, M. J., Benscoter, B., Turetsky, M., ...  
 981 Banda, E. (2017). Mapping boreal peatland ecosystem types from multitemporal radar and  
 982 optical satellite imagery. *Canadian Journal of Forest Research*, 47(4), 545–559.  
 983 <https://doi.org/10.1139/cjfr-2016-0192>
- 984 Bourgeau-Chavez, L. L., Graham, J. A., Endres, S., French, N. H. F., Battaglia, M., Hansen, D.,

- 985 & Tanzer, D. (2019). ABoVE: Ecosystem Map, Great Slave Lake Area, Northwest  
986 Territories, Canada, 1997-2011 (Version 1). ORNL Distributed Active Archive Center.  
987 <https://doi.org/10.3334/ORNLDAAC/1695>
- 988 Bridgham, S. D., Cadillo-Quiroz, H., Keller, J. K., & Zhuang, Q. (2013). Methane emissions  
989 from wetlands: biogeochemical, microbial, and modeling perspectives from local to global  
990 scales. *Global Change Biology*, 19(5), 1325–1346. <https://doi.org/10.1111/gcb.12131>
- 991 Brown, J., Ferrians, O., Heginbottom, J. A., and Melnikov E. (2002). Circum-Arctic Map of  
992 Permafrost and Ground-Ice Conditions, Version 2 [Data set]. NSIDC.  
993 <https://doi.org/10.7265/SKBG-KF16>
- 994 Burger, M., Berger, S., Spangenberg, I., & Blodau, C. (2016). Summer fluxes of methane and  
995 carbon dioxide from a pond and floating mat in a continental Canadian peatland.  
996 *Biogeosciences*, 13(12), 3777–3791. <https://doi.org/10.5194/bg-13-3777-2016>
- 997 Casas-Ruiz, J. P., Jakobsson, J., & Giorgio, P. A. del. (2021). The role of lake morphometry in  
998 modulating surface water carbon concentrations in boreal lakes. *Environmental Research*  
999 *Letters*, 16(7), 074037. <https://doi.org/10.1088/1748-9326/AC0BE3>
- 1000 Casper, P., Maberly, S. C., Hall, G. H., & Finlay, B. J. (2000). Fluxes of methane and carbon  
1001 dioxide from a small productive lake to the atmosphere. *Biogeochemistry*, 49(1), 1–19.  
1002 <https://doi.org/10.1023/A:1006269900174>
- 1003 Cheng, X., Huang, W., & Gong, J. (2014). Improved van Zyl polarimetric decomposition  
1004 lessening the overestimation of volume scattering power. *Remote Sensing*, 6(7), 6365–  
1005 6385. <https://doi.org/10.3390/rs6076365>
- 1006 Christensen, T. R., Panikov, N., Mastepanov, M., Joabsson, A., Stewart, A., Öquist, M., ...  
1007 Svensson, B. (2003). Biotic controls on CO<sub>2</sub> and CH<sub>4</sub> exchange in wetlands – a closed  
1008 environment study. *Biogeochemistry*, 64(3), 337–354.  
1009 <https://doi.org/10.1023/A:1024913730848>
- 1010 Colmer, T. D. (2003). Long-distance transport of gases in plants: a perspective on internal  
1011 aeration and radial oxygen loss from roots. *Plant, Cell and Environment*, 26(1), 17–36.  
1012 <https://doi.org/10.1046/j.1365-3040.2003.00846.x>
- 1013 Covey, K. R., & Megonigal, J. P. (2019). Methane production and emissions in trees and forests.  
1014 *New Phytologist*, 222(1), 35–51. <https://doi.org/10.1111/NPH.15624>
- 1015 Dacey, J. W. H., & Klug, M. J. (1979). Methane efflux from lake sediments through water lilies.  
1016 *Science*, 203(4386), 1253–1255. <https://doi.org/10.1126/science.203.4386.1253>
- 1017 Deemer, B. R., & Holgerson, M. A. (2021). Drivers of Methane Flux Differ Between Lakes and  
1018 Reservoirs, Complicating Global Upscaling Efforts. *Journal of Geophysical Research:*  
1019 *Biogeosciences*, 126(4), e2019JG005600. <https://doi.org/10.1029/2019JG005600>
- 1020 DelSontro, T., Boutet, L., St-Pierre, A., del Giorgio, P. A., & Prairie, Y. T. (2016). Methane

- 1021 ebullition and diffusion from northern ponds and lakes regulated by the interaction between  
1022 temperature and system productivity. *Limnology and Oceanography*, 61(S1), S62–S77.  
1023 <https://doi.org/10.1002/lno.10335>
- 1024 DelSontro, T., Beaulieu, J. J., & Downing, J. A. (2018a). Greenhouse gas emissions from lakes  
1025 and impoundments: Upscaling in the face of global change. *Limnology and Oceanography*  
1026 *Letters*, 3(3), 64–75. <https://doi.org/10.1002/lol2.10073>
- 1027 DelSontro, T., del Giorgio, P. A., & Prairie, Y. T. (2018b). No Longer a Paradox: The  
1028 Interaction Between Physical Transport and Biological Processes Explains the Spatial  
1029 Distribution of Surface Water Methane Within and Across Lakes. *Ecosystems*, 21(6), 1073–  
1030 1087. <https://doi.org/10.1007/s10021-017-0205-1>
- 1031 Denfeld, B. A., Baulch, H. M., del Giorgio, P. A., Hampton, S. E., & Karlsson, J. (2018). A  
1032 synthesis of carbon dioxide and methane dynamics during the ice-covered period of  
1033 northern lakes. *Limnology and Oceanography Letters*, 3(3), 117–131.  
1034 <https://doi.org/10.1002/LOL2.10079>
- 1035 Desrosiers, K., DelSontro, T., & del Giorgio, P. A. (2022). Disproportionate Contribution of  
1036 Vegetated Habitats to the CH<sub>4</sub> and CO<sub>2</sub> Budgets of a Boreal Lake. *Ecosystems* 2021, 1–20.  
1037 <https://doi.org/10.1007/S10021-021-00730-9>
- 1038 Dove, A., Roulet, N., Crill, P., Chanton, J., & Bourbonniere, R. (1999). Methane dynamics of a  
1039 northern boreal beaver pond. *Ecoscience*, 6(4), 577–586.
- 1040 Duarte, C. M., Kalff, J., Peters, R. H., & Peters, R. H. (1986). Patterns Biomass and Cover of  
1041 Aquatic Macrophytes in Lakes. *Canadian Journal of Fisheries and Aquatic Sciences*, 43,  
1042 1900–1908.
- 1043 Elder, C. D., Thompson, D. R., Thorpe, A. K., Chandanpurkar, H. A., Hanke, P. J., Hasson, N.,  
1044 James, S. R., Minsley, B. J., Pastick, N. J., Olefeldt, D., Anthony, K. M. W., & Miller, C. E.  
1045 (2021). Characterizing Methane Emission Hotspots From Thawing Permafrost. *Global*  
1046 *Biogeochemical Cycles*, 35(12), e2020GB006922. <https://doi.org/10.1029/2020GB006922>
- 1047 Engram, M., Walter Anthony, K. M., Sachs, T., Kohnert, K., Serafimovich, A., Grosse, G., &  
1048 Meyer, F. J. (2020). Remote sensing northern lake methane ebullition. *Nature Climate*  
1049 *Change*, 10(6), 511–517. <https://doi.org/10.1038/s41558-020-0762-8>
- 1050 Freeman, A., & Durden, S. L. (1998). A three-component scattering model for polarimetric SAR  
1051 data. *IEEE Transactions on Geoscience and Remote Sensing*.  
1052 <https://doi.org/10.1109/36.673687>
- 1053 Ganju, N. K., Defne, Z., Kirwan, M. L., Fagherazzi, S., D’Alpaos, A., & Carniello, L. (2017).  
1054 Spatially integrative metrics reveal hidden vulnerability of microtidal salt marshes. *Nature*  
1055 *Communications* 2017 8:1, 8(1), 1–7. <https://doi.org/10.1038/ncomms14156>
- 1056 Ghirardi, N., Bolpagni, R., Bresciani, M., Valerio, G., Pilotti, M., & Giardino, C. (2019).  
1057 Spatiotemporal dynamics of submerged aquatic vegetation in a deep lake from sentinel-2

- 1058 data. *Water*, 11(3), 1–14. <https://doi.org/10.3390/w11030563>
- 1059 Hastie, A., Lauerwald, R., Weyhenmeyer, G., Sobek, S., Verpoorter, C., & Regnier, P. (2018).  
1060 CO<sub>2</sub> evasion from boreal lakes: Revised estimate, drivers of spatial variability, and future  
1061 projections. *Global Change Biology*, 24(2), 711–728. <https://doi.org/10.1111/GCB.13902>
- 1062 Hess, L. L., Melack, J. M., & Simonett, D. S. (1990). Radar detection of flooding beneath the  
1063 canopy a review. *International Journal of Remote Sensing*, 11(7), 1313–1325.
- 1064 Holgerson, M. A., & Raymond, P. A. (2016). Large contribution to inland water CO<sub>2</sub> and CH<sub>4</sub>  
1065 emissions from very small ponds. *Nature Geoscience*, 9(3), 222–226.  
1066 <https://doi.org/10.1038/ngeo2654>
- 1067 Hondula, K. L., Jones, C. N., & Palmer, M. A. (2021). Effects of seasonal inundation on methane  
1068 fluxes from forested freshwater wetlands. *Environmental Research Letters*, 16(8), 084016.  
1069 <https://doi.org/10.1088/1748-9326/AC1193>
- 1070 Huttunen, J. T., Alm, J., Liikanen, A., Juutinen, S., Larmola, T., Hammar, T., ... Martikainen, P.  
1071 J. (2003). Fluxes of methane, carbon dioxide and nitrous oxide in boreal lakes and potential  
1072 anthropogenic effects on the aquatic greenhouse gas emissions. *Chemosphere*, 52, 609–621.  
1073 [https://doi.org/10.1016/S0045-6535\(03\)00243-1](https://doi.org/10.1016/S0045-6535(03)00243-1)
- 1074 Jammet, M., Crill, P., Dengel, S., & Friborg, T. (2015). Large methane emissions from a  
1075 subarctic lake during spring thaw: Mechanisms and landscape significance. *Journal of*  
1076 *Geophysical Research: Biogeosciences*, 120(11), 2289–2305.  
1077 <https://doi.org/10.1002/2015JG003137>
- 1078 Jansen, J., Thornton, B. F., Cortés, A., Snöälöv, J., Wik, M., MacIntyre, S., & Crill, P. M. (2020a).  
1079 Drivers of diffusive CH<sub>4</sub> emissions from shallow subarctic lakes on daily to multi-year  
1080 timescales. *Biogeosciences*, 17(7), 1911–1932. <https://doi.org/10.5194/bg-17-1911-2020>
- 1081 Jansen, J., Thornton, B. F., Wik, M., MacIntyre, S., & Crill, P. M. (2020b). Temperature Proxies  
1082 as a Solution to Biased Sampling of Lake Methane Emissions. *Geophysical Research*  
1083 *Letters*, 47(14). <https://doi.org/10.1029/2020GL088647>
- 1084 Jensen, D., Cavanaugh, K. C., Simard, M., Christensen, A., Rovai, A., & Twilley, R. (2021).  
1085 Aboveground biomass distributions and vegetation composition changes in Louisiana's  
1086 Wax Lake Delta. *Estuarine, Coastal and Shelf Science*, 250, 107139.  
1087 <https://doi.org/10.1016/j.ecss.2020.107139>
- 1088 Joabsson, A., Christensen, T. R., & Wallén, B. (1999). Vascular plant controls on methane  
1089 emissions from northern peatforming wetlands. *Trends in Ecology & Evolution*, 14(10),  
1090 385–388. [https://doi.org/10.1016/S0169-5347\(99\)01649-3](https://doi.org/10.1016/S0169-5347(99)01649-3)
- 1091 Johnston, S. E., Striegl, R. G., Bogard, M. J., Dornblaser, M. M., Butman, D. E., Kellerman, A.  
1092 M., ... Spencer, R. G. M. (2020). Hydrologic connectivity determines dissolved organic  
1093 matter biogeochemistry in northern high-latitude lakes. *Limnology and Oceanography*  
1094 *Oceanography*. <https://doi.org/10.1002/lno.11417>

- 1095 Jordahl, Kelsey, Joris Van den Bossche, Martin Fleischmann, James McBride, Jacob  
1096 Wasserman, Adrian Garcia Badaracco, Jeffrey Gerard, Alan D. Snow, Jeff Tratner,  
1097 Matthew Perry, Carson Farmer, Geir Arne Hjelle, Micah Cochran, Sean Gillies, Lucas  
1098 Culbertson, Matt Bartos, Brendan Ward, Giacomo Caria, Mike Taves, ... Leah Wasser.  
1099 (2021). geopandas/geopandas: v0.10.2 (v0.10.2). Zenodo.  
1100 <https://doi.org/10.5281/zenodo.5573592>
- 1101 Juutinen, S., Alm, J., Larmola, T., Huttunen, J. T., Morero, M., Martikainen, P. J., & Silvola, J.  
1102 (2003). Major implication of the littoral zone for methane release from boreal lakes. *Global*  
1103 *Biogeochemical Cycles*, 17(4). <https://doi.org/10.1029/2003gb002105>
- 1104 Kankaala, P., Huotari, J., Tulonen, T., & Ojala, A. (2013). Lake-size dependent physical forcing  
1105 drives carbon dioxide and methane effluxes from lakes in a boreal landscape. *Limnology*  
1106 *and Oceanography*, 58(6), 1915–1930. <https://doi.org/10.4319/lo.2013.58.6.1915>
- 1107 Kankaala, P., Kaki, T., Makela, S., Ojala, A., Pajunen, H., & Arvola, L. (2005). Methane efflux  
1108 in relation to plant biomass and sediment characteristics in stands of three common  
1109 emergent macrophytes in boreal mesoeutrophic lakes. *Global Change Biology*, 11(1), 145–  
1110 153. <https://doi.org/10.1111/j.1365-2486.2004.00888.x>
- 1111 McKenzie Kuhn, Ruth Varner, David Bastviken, Patrick Crill, Sally MacIntyre, et al. 2021a.  
1112 BAWLD-CH4: Methane Fluxes from Boreal and Arctic Ecosystems. Arctic Data Center.  
1113 [doi:10.18739/A2DN3ZX1R](https://doi.org/10.18739/A2DN3ZX1R).
- 1114 Kuhn, M. A., Varner, R. K., Bastviken, D., Crill, P., Macintyre, S., Turetsky, M., Anthony, K.  
1115 W., Mcguire, A. D., & Olefeldt, D. (2021b). BAWLD-CH 4 : a comprehensive dataset of  
1116 methane fluxes from boreal and arctic ecosystems. *Earth Syst. Sci. Data*, 13, 5151–5189.  
1117 <https://doi.org/10.5194/essd-13-5151-2021>
- 1118 Kyzivat, E. D., Smith, L. C., Pitcher, L. H., Arvesen, J., Pavelsky, T. M., Cooley, S. W., & Topp,  
1119 S. (2018). ABoVE: AirSWOT Color-Infrared Imagery Over Alaska and Canada, 2017.  
1120 ORNL Distributed Active Archive Center. <https://doi.org/10.3334/ORNLDAAAC/1643>
- 1121 Kyzivat, E. D., Smith, L. C., Pitcher, L. H., Fayne, J. V., Cooley, S. W., Cooper, M. G., ...  
1122 Pavelsky, T. M. (2019). A high-resolution airborne color-infrared camera water mask for  
1123 the NASA ABoVE campaign. *Remote Sensing*, 11, 1–28.  
1124 <https://doi.org/10.3390/rs11182163>
- 1125 Kyzivat, E. D., Smith, L. C., Pitcher, L. H., Fayne, J. V., Cooley, S. W., Cooper, M. G., Topp, S.,  
1126 Langhorst, T., Harlan, M. E., Gleason, C. J., & Pavelsky, T. M. (2020). ABoVE: AirSWOT  
1127 Water Masks from Color-Infrared Imagery over Alaska and Canada, 2017 (Version 1).  
1128 ORNL Distributed Active Archive Center. <https://doi.org/10.3334/ORNLDAAAC/1707>
- 1129 Kyzivat, E. D., Smith, L. C., Huang, C., Wang, C., Langhorst, T., Fayne, J. V., Harlan, M.E.,  
1130 Ishitsuka, Y., Feng, D., Dolan, W., Pitcher, L.H, Pavelsky, T. M. (2021a). ABoVE: Lake  
1131 and Wetland Classification from L-band SAR, Alaska and Canada, 2017-2019. ORNL  
1132 Distributed Active Archive Center. <https://doi.org/10.3334/ORNLDAAAC/1883>

- 1133 Kyzivat, E., F. Garcia Tigreros, T. Langhorst, J.V. Fayne, M.E. Harlan, Y. Ishitsuka, D. Feng,  
1134 K.P. Wickland, M.M. Dornblaser, R.G. Striegl, D.E. Butman, and C.J. Gleason. 2021b.  
1135 Methane and carbon dioxide fluxes from vegetated and open water zones of lakes in the  
1136 Peace-Athabasca Delta, Alberta, Canada, 2019 ver 1. Environmental Data Initiative.  
1137 <https://doi.org/10.6073/pasta/1e0cadadd8024c8fab692ee21dc1f57> (Accessed 2022-03-04).
- 1138 Laanbroek, H. J. (2009). Methane emission from natural wetlands: interplay between emergent  
1139 macrophytes and soil microbial processes. A mini-review.
- 1140 Langenegger, T., Vachon, D., Donis, D., & McGinnis, D. F. (2019). What the bubble knows:  
1141 Lake methane dynamics revealed by sediment gas bubble composition. *Limnology and*  
1142 *Oceanography*, 64(4), 1526–1544. <https://doi.org/10.1002/LNO.11133>
- 1143 Larmola, T., Alm, J., Juutinen, S., Huttunen, J. T., Martikainen, P. J., & Silvola, J. (2004).  
1144 Contribution of vegetated littoral zone to winter fluxes of carbon dioxide and methane from  
1145 boreal lakes. *J. Geophys. Res*, 109. <https://doi.org/10.1029/2004JD004875>
- 1146 Lehner, B., & Döll, P. (2004). Development and validation of a global database of lakes,  
1147 reservoirs and wetlands. *Journal of Hydrology*, 296, 1–22.  
1148 <https://doi.org/10.1016/j.jhydrol.2004.03.028>
- 1149 Li, M., Peng, C., Zhu, Q., Zhou, X., Yang, G., Song, X., & Zhang, K. (2020). The significant  
1150 contribution of lake depth in regulating global lake diffusive methane emissions. *Water*  
1151 *Research*, 172, 115465. <https://doi.org/10.1016/j.watres.2020.115465>
- 1152 Loken, L. C., Crawford, J. T., Schramm, P. J., Stadler, P., Desai, A. R., & Stanley, E. H. (2019).  
1153 Large Spatial and Temporal Variability of Carbon Dioxide and Methane in a Eutrophic  
1154 Lake. *Journal of Geophysical Research: Biogeosciences*, 124(7), 2248–2266.  
1155 <https://doi.org/10.1029/2019JG005186>
- 1156 Mäkelä, S., Huitu, E., & Arvola, L. (2004). Spatial patterns in aquatic vegetation composition  
1157 and environmental covariates along chains of lakes in the Kokemäenjoki watershed (S.  
1158 Finland). *Aquatic Botany*, 80(4), 253–269. <https://doi.org/10.1016/j.aquabot.2004.08.006>
- 1159 Melton, J. R., Wania, R., Hodson, E. L., Poulter, B., Ringeval, B., Spahni, R., ... Kaplan, J. O.  
1160 (2013). Present state of global wetland extent and wetland methane modelling: conclusions  
1161 from a model inter-comparison project (WETCHIMP). *Biogeosciences*, 10, 753–788.  
1162 <https://doi.org/10.5194/bg-10-753-2013>
- 1163 Messenger, M. L., Lehner, B., Grill, G., Nedeva, I., & Schmitt, O. (2016). Estimating the volume  
1164 and age of water stored in global lakes using a geo-statistical approach. *Nature*  
1165 *Communications*, 7, 1–11. <https://doi.org/10.1038/ncomms13603>
- 1166 Michmerhuizen, C. M., Striegl, R. G., & McDonald, M. E. (1996). Potential methane emission  
1167 from north-temperate lakes following ice melt. *Limnology and Oceanography*, 41(5), 985–  
1168 991. <https://doi.org/10.4319/lo.1996.41.5.0985>
- 1169 Miller, C., Griffith, C. P., Goetz, S. J., Hoy, E. E., Pinto, N., McCubbin, I. B., ... Margolis, H. A.

- 1170 (2019). An overview of ABoVE airborne campaign data acquisitions and science  
1171 opportunities. *Environmental Research Letters*, 14(8). [https://doi.org/10.1088/1748-](https://doi.org/10.1088/1748-9326/ab0d44)  
1172 9326/ab0d44
- 1173 NASA/JPL. (2017-2019). UAVSAR\_POLSAR [Data set]. NASA Alaska Satellite Facility  
1174 DAAC. <https://doi.org/10.5067/7PEQV8SVR4DM>
- 1175 Natchimuthu, S., Sundgren, I., Gålfalk, M., Klemedtsson, L., Crill, P., Danielsson, Å., &  
1176 Bastviken, D. (2016). Spatio-temporal variability of lake CH<sub>4</sub> fluxes and its influence on  
1177 annual whole lake emission estimates. *Limnology and Oceanography*, 61(S1), S13–S26.  
1178 <https://doi.org/10.1002/lno.10222>
- 1179 Nelson, S. A. C., Cheruvilil, K. S., & Soranno, P. A. (2006). Satellite remote sensing of  
1180 freshwater macrophytes and the influence of water clarity. *Aquatic Botany*, 85(4), 289–298.  
1181 <https://doi.org/10.1016/j.aquabot.2006.06.003>
- 1182 David Olefeldt, Mikael Hovemyr, McKenzie Kuhn, David Bastviken, Theodore Bohn, et al.  
1183 2021. The fractional land cover estimates from the Boreal-Arctic Wetland and Lake Dataset  
1184 (BAWLD), 2021b. Arctic Data Center. <https://doi.org/10.18739/A2C824F9X>
- 1185 Olefeldt, D., Hovemyr, M., Kuhn, M. A., Bastviken, D., Bohn, T. J., Connolly, J., Crill, P.,  
1186 Euskirchen, E. S., Finkelstein, S. A., Genet, H., Grosse, G., Harris, L. I., Heffernan, L.,  
1187 Helbig, M., Hugelius, G., Hutchins, R., Juutinen, S., Lara, M. J., Malhotra, A., ... Watts, J.  
1188 D. (2021a). The Boreal-Arctic Wetland and Lake Dataset (BAWLD) D. Olefeldt et al.: The  
1189 Boreal-Arctic Wetland and Lake Dataset. *Earth Syst. Sci. Data*, 13, 5127–5149.  
1190 <https://doi.org/10.5194/essd-13-5127-2021>
- 1191 Parks Canada. (2019). *Wood Buffalo National Park World Heritage Site Action Plan* (Cat. No.:  
1192 978-0-660-27537-6). Retrieved from [https://pcacdn.azureedge.net/-/media/pn-](https://pcacdn.azureedge.net/-/media/pn-nt/woodbuffalo/2021-changes/02_11-action-plan-PDFs/WoodBuffalo-WHS-Action-Plan_EN.pdf)  
1193 [np/nt/woodbuffalo/2021-changes/02\\_11-action-plan-PDFs/WoodBuffalo-WHS-Action-](https://pcacdn.azureedge.net/-/media/pn-nt/woodbuffalo/2021-changes/02_11-action-plan-PDFs/WoodBuffalo-WHS-Action-Plan_EN.pdf)  
1194 [Plan\\_EN.pdf](https://pcacdn.azureedge.net/-/media/pn-nt/woodbuffalo/2021-changes/02_11-action-plan-PDFs/WoodBuffalo-WHS-Action-Plan_EN.pdf)
- 1195 Pavelsky, T. M., & Smith, L. C. (2008). Remote sensing of hydrologic recharge in the Peace-  
1196 Athabasca Delta, Canada. *Geophysical Research Letters*.  
1197 <https://doi.org/10.1029/2008GL033268>
- 1198 Rey-Sanchez, A. C., Morin, T. H., Stefanik, K. C., Wrighton, K., & Bohrer, G. (2018).  
1199 Determining total emissions and environmental drivers of methane flux in a Lake Erie  
1200 estuarine marsh. *Ecological Engineering*, 114, 7–15.  
1201 <https://doi.org/10.1016/j.ecoleng.2017.06.042>
- 1202 Ribaudo, C., Bartoli, M., Longhi, D., Castaldi, S., Neubauer, S. C., & Viaroli, P. (2012). CO<sub>2</sub>  
1203 and CH<sub>4</sub> fluxes across a *Nuphar lutea* (L.) Sm. stand. *Journal of Limnology*, 71(1), 200–  
1204 210.
- 1205 Rosentreter, J. A., Borges, A. v, Deemer, B. R., Holgerson, M. A., Liu, S., Song, C., Melack, J.,  
1206 Raymond, P. A., Duarte, C. M., Allen, G. H., Olefeldt, D., Poulter, B., Battin, T. I., & Eyre,  
1207 B. D. (2021). Half of global methane emissions come from highly variable aquatic

- 1208 ecosystem sources. *Nature Geoscience*. <https://doi.org/10.1038/s41561-021-00715-2>
- 1209 Saunio, M., Stavert, A. R., Poulter, B., Bousquet, P., Canadell, J. G., Jackson, R. B., ... Zhuang,  
1210 Q. (2020). The Global Methane Budget 2000–2017. *Earth Syst. Sci. Data*, *12*, 1561–1623.  
1211 <https://doi.org/10.5194/essd-12-1561-2020>
- 1212 Schmiedeskamp, M., Stephanie, L., Praetzel, E., Bastviken, D., & Knorr, K.-H. (2021). Whole-  
1213 lake methane emissions from two temperate shallow lakes with fluctuating water levels:  
1214 Relevance of spatiotemporal patterns. *Limnol. Oceanogr*, *9999*, 1–15.  
1215 <https://doi.org/10.1002/lno.11764>
- 1216 Seekell, D., Cael, B., Norman, S., & Byström, P. (2021). Patterns and Variation of Littoral  
1217 Habitat Size Among Lakes. *Geophysical Research Letters*, *48*(20), e2021GL095046.  
1218 <https://doi.org/10.1029/2021GL095046>
- 1219 Simard, M., Riel, B. V., Denbina, M., & Hensley, S. (2016). Radiometric Correction of Airborne  
1220 Radar Images over Forested Terrain with Topography. *IEEE Transactions on Geoscience  
1221 and Remote Sensing*, *54*(8), 4488–4500. <https://doi.org/10.1109/TGRS.2016.2543142>
- 1222 Slaymaker, O. (2016). *Landscapes and Landforms of Western Canada*. Springer International  
1223 Publishing.
- 1224 Smith, L. K., & Lewis, W. M. (1992). Seasonality of methane emissions from five lakes and  
1225 associated wetlands of the Colorado Rockies. *Global Biogeochemical Cycles*, *6*(4), 323–  
1226 338. <https://doi.org/10.1029/92GB02016>
- 1227 Smith, V. H., & Wallsten, M. (1986). Prediction of emergent and floating-leaved macrophyte  
1228 cover in Central Swedish lakes. *Canadian Journal of Fisheries and Aquatic Sciences*,  
1229 *43*(12), 2519–2523. <https://doi.org/10.1139/f86-311>
- 1230 Spence, C., & Woo, M. (2006). Hydrology of subarctic Canadian Shield: heterogeneous  
1231 headwater basins. *Journal of Hydrology*, *317*(1–2), 138–154.  
1232 <https://doi.org/10.1016/J.JHYDROL.2005.05.014>
- 1233 Stephanie, L., Praetzel, E., Plenter, N., Schilling, S., Schmiedeskamp, M., Broll, G., ...  
1234 Praetzel@uni-Muenster, L. De. (2020). Organic matter and sediment properties determine  
1235 in-lake variability of sediment CO<sub>2</sub> and CH<sub>4</sub> production and emissions of a small and  
1236 shallow lake. *Biogeosciences*, *17*, 5057–5078. <https://doi.org/10.5194/bg-17-5057-2020>
- 1237 Striegl, R. G., Dornblaser, M. M., McDonald, C. P., Rover, J. R., & Stets, E. G. (2012). Carbon  
1238 dioxide and methane emissions from the Yukon River system. *Global Biogeochemical  
1239 Cycles*, *26*(4). <https://doi.org/10.1029/2012GB004306>
- 1240 Striegl, R. G., & Michmerhuizen, C. M. (1998). Hydrologic influence on methane and carbon  
1241 dioxide dynamics at two north-central Minnesota lakes. *Limnology and Oceanography*,  
1242 *43*(7), 1519–1529. <https://doi.org/10.4319/lo.1998.43.7.1519>
- 1243 Ström, L., Mastepanov, M., & Christensen, T. R. (2005). Species-specific Effects of Vascular

- 1244 Plants on Carbon Turnover and Methane Emissions from Wetlands. *Biogeochemistry*,  
1245 75(1), 65–82. <https://doi.org/10.1007/s10533-004-6124-1>
- 1246 Thornton, B. F., Wik, M., & Crill, P. M. (2016). Double-counting challenges the accuracy of  
1247 high-latitude methane inventories. *Geophysical Research Letters*, 43(24), 12,569–12,577.  
1248 <https://doi.org/10.1002/2016GL071772>
- 1249 Timoney, K. P. (2013). *The Peace-Athabasca Delta: Portrait of a Dynamic Ecosystem*.  
1250 Edmonton: University of Alberta Press.
- 1251 Töyrä, J., & Pietroniro, A. (2005). Towards operational monitoring of a northern wetland using  
1252 geomatics-based techniques. *Remote Sensing of Environment*, 97(2), 174–191.  
1253 <https://doi.org/10.1016/J.RSE.2005.03.012>
- 1254 Tranvik, L. J., Downing, J. A., Cotner, J. B., Loiselle, S. A., Striegl, R. G., Ballatore, T. J., ...  
1255 Weyhenmeyer, G. A. (2009). Lakes and reservoirs as regulators of carbon cycling and  
1256 climate. *Limnology and Oceanography*, 54(6part2), 2298–2314.  
1257 [https://doi.org/10.4319/lo.2009.54.6\\_part\\_2.2298](https://doi.org/10.4319/lo.2009.54.6_part_2.2298)
- 1258 Ulander, L. M. H. (1996). Radiometric slope correction of synthetic-aperture radar images. *IEEE*  
1259 *Transactions on Geoscience and Remote Sensing*, 34(5), 1115–1122.  
1260 <https://doi.org/10.1109/36.536527>
- 1261 Verpoorter, C., Kutser, T., Seekell, D. A., & Tranvik, L. J. (2014). A global inventory of lakes  
1262 based on high-resolution satellite imagery. *Geophysical Research Letters*, 41(18), 6396–  
1263 6402. <https://doi.org/10.1002/2014GL060641>
- 1264 Villa, J. A., Ju, Y., Yazbeck, T., Waldo, S., Wrighton, K. C., & Bohrer, G. (2021). Ebullition  
1265 dominates methane fluxes from the water surface across different ecohydrological patches  
1266 in a temperate freshwater marsh at the end of the growing season. *Science of the Total*  
1267 *Environment*, 767, 144498. <https://doi.org/10.1016/j.scitotenv.2020.144498>
- 1268 Wang, J. A., Sulla-menashe, D., Woodcock, C. E., Sonnentag, O., Keeling, R. F., & Friedl, M.  
1269 A. (2019). ABoVE: Landsat-derived Annual Dominant Land Cover Across ABoVE Core  
1270 Domain, 1984-2014. ORNL Distributed Active Archive Center.  
1271 <https://doi.org/10.3334/ORNLDAAAC/1691>
- 1272 Wang, J. A., Sulla-Menashe, D., Woodcock, C. E., Sonnentag, O., Keeling, R. F., & Friedl, M.  
1273 A. (2019). Extensive land cover change across Arctic–Boreal Northwestern North America  
1274 from disturbance and climate forcing. *Global Change Biology*, 00, 1–16.  
1275 <https://doi.org/10.1111/gcb.14804>
- 1276 Ward, E. M., & Gorelick, S. M. (2018). Drying drives decline in muskrat population in the  
1277 Peace-Athabasca Delta, Canada. *Environmental Research Letters*, 13, 124026.  
1278 <https://doi.org/10.1088/1748-9326/aaf0ec>
- 1279 West, W. E., Creamer, K. P., & Jones, S. E. (2016). Productivity and depth regulate lake  
1280 contributions to atmospheric methane. *Limnology and Oceanography*, 61(S1), S51–S61.

- 1281 <https://doi.org/10.1002/LNO.10247>
- 1282 Wetzel, R. G. (1990). Land-water interfaces: Metabolic and limnological regulators. *Verh.*  
1283 *Internat. Verein. Limnol.*, 24(September), 6–24.
- 1284 Wetzel, R. G. (2001). *Limnology: Lake and River Ecosystems* (Third). Boston: Academic Press.
- 1285 Wik, M., Crill, P. M., Varner, R. K., & Bastviken, D. (2013). Multiyear measurements of  
1286 ebullitive methane flux from three subarctic lakes. *Journal of Geophysical Research:*  
1287 *Biogeosciences*, 118(3), 1307–1321. <https://doi.org/10.1002/jgrg.20103>
- 1288 Wik, M., Varner, R. K., Anthony, K. W., MacIntyre, S., & Bastviken, D. (2016a). Climate-  
1289 sensitive northern lakes and ponds are critical components of methane release. *Nature*  
1290 *Geoscience*, 9(2), 99–105. <https://doi.org/10.1038/ngeo2578>
- 1291 Wik, M., Thornton, B. F., Bastviken, D., Uhlbäck, J., & Crill, P. M. (2016b). Biased sampling of  
1292 methane release from northern lakes: A problem for extrapolation. *Geophysical Research*  
1293 *Letters*, 43(3), 1256–1262. <https://doi.org/10.1002/2015GL066501>
- 1294 Wolfe, B. B., Hall, R. I., Last, W. M., Edwards, T. W. D., English, M. C., Karst-Riddoch, T. L.,  
1295 ... Palmi, R. (2006). Reconstruction of multi-century flood histories from oxbow lake  
1296 sediments, Peace-Athabasca Delta, Canada. *Hydrological Processes*, 20(19), 4131–4153.  
1297 <https://doi.org/10.1002/hyp.6423>
- 1298 Zhang, B., Tian, H., Lu, C., Chen, G., Pan, S., Anderson, C., & Poulter, B. (2017). Methane  
1299 emissions from global wetlands: An assessment of the uncertainty associated with various  
1300 wetland extent data sets. *Atmospheric Environment*, 165, 310–321.  
1301 <https://doi.org/10.1016/J.ATMOSENV.2017.07.001>
- 1302 Zhang, S., Foerster, S., Medeiros, P., de Araújo, J. C., & Waske, B. (2018). Effective water  
1303 surface mapping in macrophyte-covered reservoirs in NE Brazil based on TerraSAR-X time  
1304 series. *International Journal of Applied Earth Observation and Geoinformation*, 69, 41–55.  
1305 <https://doi.org/10.1016/j.jag.2018.02.014>
- 1306 Zhang, Y., Jeppesen, E., Liu, X., Qin, B., Shi, K., Zhou, Y., ... Deng, J. (2017). Global loss of  
1307 aquatic vegetation in lakes. *Earth-Science Reviews*, 173, 259–265.  
1308 <https://doi.org/https://doi.org/10.1016/j.earscirev.2017.08.013>
- 1309 Zhang, Z., Ni, W., Sun, G., Huang, W., Ranson, K. J., Cook, B. D., & Guo, Z. (2017). Biomass  
1310 retrieval from L-band polarimetric UAVSAR backscatter and PRISM stereo imagery.  
1311 *Remote Sensing of Environment*, 194, 331–346. <https://doi.org/10.1016/J.RSE.2017.03.034>
- 1312 Zhang, Z., Fluet-Chouinard, E., Jensen, K., McDonald, K., Hugelius, G., Gumbrecht, T., ...  
1313 Poulter, B. (2021). Development of the global dataset of Wetland Area and Dynamics for  
1314 Methane Modeling (WAD2M). *Earth Syst. Sci. Data*, 13. [https://doi.org/10.5194/essd-13-](https://doi.org/10.5194/essd-13-2001-2021)  
1315 [2001-2021](https://doi.org/10.5194/essd-13-2001-2021)